

**NASCTN Report 6**  
**NIST Technical Note 2056**

**LTE Handset Emissions: Radiation Pattern  
Measurements  
Final Test Report**

Robert D. Horansky  
Jason B. Coder  
John M. Ladbury

This publication is available free of charge from:  
<https://doi.org/10.6028/NIST.TN.2056>



## National Advanced Spectrum and Communications Test Network (NASCTN)

The mission of the National Advanced Spectrum and Communications Test Network (NASCTN) is to provide, through its members, robust test processes and validated measurement data necessary to develop, evaluate and deploy spectrum sharing technologies that can increase access to the spectrum by both federal agencies and non-federal spectrum users.

NASCTN was formed to provide a single focal point for engaging industry, academia, and other government agencies on advanced spectrum technologies, including testing, measurement, validation, and conformity assessment. The National Institute of Standards and Technology (NIST) hosts the NASCTN capability at the Department of Commerce Boulder Laboratories in Boulder, Colorado.

NASCTN is a membership organization under a charter agreement. Members

- Make available, in accordance with their organization's rules policies and regulations, engineering capabilities and test facilities, with typical consideration for cost.
- Coordinate their efforts to identify, develop and test spectrum sharing ideas, concepts and technology to support the goal of advancing more efficient and effective spectrum sharing.
- Make available information related to spectrum sharing, considering requirements for the protection of intellectual property, national security, and other organizational controls, and, to the maximum extent possible, allow the publication of NASCTN test results.
- Ensure all spectrum sharing efforts are identified to other interested members.

Current charter members are:

- Department of Defense Chief Information Officer (DoD CIO)
- National Institute of Standards and Technology (NIST)
- National Oceanic and Atmospheric Administration (NOAA)
- National Science Foundation (NSF)
- National Telecommunications and Information Administration (NTIA)



NASCTN Report 6

NIST Technical Note 2056

# LTE Handset Emissions: Radiation Pattern Measurements Final Test Report

Robert D. Horansky

Jason B. Coder

John M. Ladbury

*RF Technology Division*

*Communications Technology Laboratory, NIST*

August 16, 2019



U.S. Department of Commerce

*Wilbur L. Ross, Jr., Secretary*

National Institute of Standards and Technology

*Walter Copan, NIST Director and Undersecretary of Commerce for Standards and Technology*

Certain commercial entities, equipment, or materials may be identified in this document in order to describe an experimental procedure or concept adequately. Such identification is not intended to imply recommendation or endorsement by the National Institute of Standards and Technology, nor is it intended to imply that the entities, materials, or equipment are necessarily the best available for the purpose.

**National Institute of Standards and Technology Technical Note 2056**  
**Natl. Inst. Stand. Technol. Tech. Note 2056, (August 2019)**  
**CODEN: NTNOEF**

**This publication is available free of charge from:**  
**<https://doi.org/10.6028/NIST.TN.2056>**

# Acknowledgments

The authors express their thanks to the Defense Spectrum Organization (DSO) for the trust and confidence they have placed in National Advanced Spectrum and Communications Test Network to conduct these measurements and document the results that will be used by multiple organizations conducting research on 3rd generation partnership's long term evolution protocols.

The authors also thank the National Institute of Standards and Technology Radio Frequency Division for their support in this measurement effort for NASCTN.

# Abstract

This report describes work that measured the three dimensional emission patterns for a variety of user equipment (UE) handset devices operating on long-term evolution (LTE) protocols. This effort was part of a National Advanced Spectrum and Communication Test Network (NASCTN) project sponsored by the Defense Spectrum Organization (DSO) to investigate the factors that influence aggregate LTE UE emissions in the advanced wireless service 3 (AWS-3) band and the sensitivity of the emissions to those factors. The work presented in this technical note supported the NASCTN's "Aggregate LTE: Characterizing UE Emissions" project outcomes by ensuring the best orientation and associated uncertainty for transmission was known for each UE tested. Due to the potential benefit to the broader spectrum community, this work is being released as a stand-alone technical report as well as an appendix to the final "Aggregate LTE: Characterizing UE Emissions" technical report

# Contents

Acknowledgments . . . . .	ii
<b>Abstract</b>	<b>iii</b>
Preface . . . . .	iii
List of Acronyms . . . . .	v
List of Figures . . . . .	vii
List of Tables . . . . .	ix
<b>1 Introduction</b>	<b>1</b>
1.1 Objective . . . . .	2
1.2 Scope . . . . .	2
1.3 Background . . . . .	2
<b>2 UE Antenna Pattern Measurements and Calculations</b>	<b>5</b>
2.1 Introduction . . . . .	5
2.2 Experiment Setup . . . . .	6
2.2.1 Total Radiated Power . . . . .	11
2.2.2 Uncertainties due to UE Orientation . . . . .	12
<b>3 Measurement Results</b>	<b>15</b>
3.1 Fixture . . . . .	15
3.1.1 Polystyrene Mount . . . . .	15
3.1.2 Effect of Three-Dimensional Rotation Fixture . . . . .	18
3.2 Full Three-Dimensional Patterns . . . . .	20
<b>4 Discussion</b>	<b>31</b>
4.1 Dipole Antenna Approximation . . . . .	31
4.2 Distribution of EIRP . . . . .	32
<b>5 Conclusions</b>	<b>34</b>
5.1 Summary . . . . .	34
<b>A Data Acquisition Flow</b>	<b>35</b>
<b>Bibliography</b>	<b>38</b>

# Acronyms

<b>AWS3</b>	advanced wireless services 3
<b>CSMAC</b>	Commerce Spectrum management and Advisory Committee
<b>DISA</b>	Defense Information Systems Agency
<b>DoD</b>	Department of Defense
<b>DSO</b>	Defense Spectrum Organization
<b>EEPAC</b>	early entry portal analysis capability
<b>EIRP</b>	effective isotropic radiated power
<b>FCC</b>	Federal Communications Commission
<b>LTE</b>	long-term evolution
<b>NASCTN</b>	National Advanced Spectrum and Communications Test Network
<b>NBIT</b>	NIST Broadband Interoperability Test
<b>NIST</b>	National Institute of Standards and Technology
<b>NTIA</b>	National Telecommunications and Information Administration
<b>OTA</b>	over the air
<b>PRB</b>	physical resource block
<b>RF</b>	radio frequency
<b>SRF</b>	spectrum relocation fund
<b>SSTD</b>	spectrum sharing test and demonstration
<b>TRP</b>	total radiated power
<b>UE</b>	user equipment
<b>UL</b>	uplink
<b>VNA</b>	vector network analyzer



# List of Figures

1.1	Description of the AWS-3 Band. . . . .	3
2.1	Schematic representation of the anechoic chamber, measurement antenna, turntable, rotator, and UE. . . . .	7
2.2	Photograph of the anechoic chamber, measurement antenna, turntable, rotator, and UE. . . . .	8
2.3	Schematic of path loss measurement setup. . . . .	9
2.4	Measured EIRP versus $\theta$ at several orientations of $\phi$ comparing connection of power cable . . . . .	13
2.5	Histogram of EIRP from repeat measurements. . . . .	13
2.6	Histogram of EIRP from repeat measurements with charging cable. . . . .	14
3.1	Sketch showing the orientation of the landscape-oriented UE. . . . .	16
3.2	Landscape orientation antenna patterns from UEs A, B, and C. . . . .	17
3.3	Schematic of landscape UE orientation with horizontally polarized measurement antenna. . . . .	17
3.4	Radiation patterns with UE in landscape orientation and horizontally polarized measurement antenna. . . . .	18
3.5	Sketch of portrait-oriented UE . . . . .	19
3.6	Radiation patterns from portrait-oriented UEs. . . . .	19
3.7	Determination of effect of acrylic mounting block on radiation pattern. . . . .	21
3.8	Sketch of bi-axial rotation fixture. . . . .	22
3.9	Plot of EIRP from UE versus turntable angle with polystyrene mount. . . . .	23
3.10	Three-dimensional radiation pattern of UE B with a slice in the $\phi$ direction at $\theta = 0.3^\circ$ . . . . .	24
3.11	Three-dimensional radiation pattern of UE B with a slice in the $\phi$ direction at $\theta = 90^\circ$ . . . . .	24
3.12	[Three-dimensional radiation pattern of UE B with a slice in the $\theta$ direction at $\phi = 0$ . . . . .	25
3.13	Three-dimensional radiation pattern of UE B with horizontally polarized measurement antenna. . . . .	26
3.14	Three-dimensional radiation pattern of UE B with horizontally polarized measurement antenna and a slice in the $\phi$ direction. . . . .	27
3.15	Three-dimensional radiation pattern of UE B with horizontally polarized measurement antenna and a cut in the $\theta$ direction. . . . .	27
3.16	Three-dimensional radiation pattern of UE B with horizontally polarized measurement antenna and a cut in the $\theta$ direction at $\phi = 90^\circ$ . . . . .	28
3.17	Comparison of three-dimensional radiation patterns from all UE's tested with vertically polarized measurement antenna. . . . .	29
3.18	Comparison of three-dimensional radiation patterns from all UE's tested with horizontally polarized measurement antenna. . . . .	30
4.1	Distribution of EIRP measured from all UE's. . . . .	32
4.2	Three-dimensional pattern of sum of horizontal and vertical polarization of UE B . . . . .	33
A.1	Flow diagram of the data acquisition software. . . . .	36



# List of Tables

2.1	Collection of LTE UEs used for the study presented here. The letter designator, approximate planar dimensions, and quantity of each UE is shown in the table. . . . .	6
2.2	Calculation of TRP From Three-Dimensional Radiation Patterns (15° steps). . . . .	11



# Chapter 1

## Introduction

The Defense Information Systems Agency (DISA) Defense Spectrum Organization (DSO) through the Spectrum Sharing Test and Development (SSTD) program proposed to the National Advanced Spectrum and Communications Test Network (NASCTN) a measurement campaign to quantitatively characterize Long Term Evolution (LTE) uplink (UL) emissions generated by User Equipment (UE) in the 1755 MHz to 1780 MHz band. DSO's intent is to develop realistic models of UE emissions. These models will be used for assessing interference to Department of Defense (DoD) systems that, for a time, will remain in the 1755 MHz to 1780 MHz band.

The test executed by NASCTN is one of a series of potential measurements designed to better understand the emissions of commercial LTE UEs, both individually and in aggregate. This project performed a series of controlled laboratory measurements over a sampling of LTE network, environmental, and use case conditions which were designed to better understand UE emissions and what parameter(s) impact these emissions. In contrast to field-based measurements with limited knowledge of network settings, laboratory measurements allowed control and manipulation of key aspects of the network and environment, giving the ability to test the sensitivity of each parameter of interest. The work included an analysis of the assumptions, measurement uncertainties, and their effects on the uncertainty of the estimated parameters.

In order to support the NASCTN project, an understanding of the three dimensional emission patterns of typical LTE UEs was needed. Current simulations use a simplistic and static representation of UE antenna patterns as an isotropic emitter which does not capture true effects nor any variation between manufacturers and models. The UE pattern measurements presented in this report allow analysis of the impact of location of the UE to emission strength and differences in radiated behavior between a sampling of UEs. This paper provides the details and results of the UE pattern measurement activity.

## 1.1 Objective

The objective of this NASCTN effort was to measure the three dimensional emission patterns of a series of sample LTE UEs as well as determine an optimized measurement geometry for the NASCTN "Aggregate LTE: Characterizing UE Emissions" project. These measurements provide insight into the effect of orientation of the UE on emissions. This directly supports the NASCTN project for DSO, but also supports the broader activities of the SSTD and the LTE community.

## 1.2 Scope

This study specifically addressed the characterization of the radiation pattern of in-band RF emissions from a collection of LTE UE handsets that span cost, physical size, and operating system. We built a test fixture for measuring the full  $4\pi$  steradians angular dependence of the UE transmission and use this measurement to inform experiment design in the LTE aggregate experiment.

## 1.3 Background

In the 2010 Presidential Memorandum on Unleashing the Wireless Broadband Revolution [1], the National Telecommunications and Information Administration (NTIA) was tasked to identify underutilized spectrum suitable for wireless broadband use. In the subsequent NTIA Fast Track Report [2], many federal bands were identified as commercially viable. From this report, the Federal Communication Commission (FCC) identified 1695 MHz to 1710 MHz, 1755 MHz to 1780 MHz, and 2155 MHz to 2180 MHz, together known as the 3rd advanced wireless services group of bands (called together Advanced Wireless Service – 3 (AWS-3)) in July 2013. The AWS-3 band is shown in Figure 1.1. The FCC adopted a Report and Order in March 2014 with allocation, technical, and licensing rules for commercial use of the AWS-3 bands [3]. The uplink blocks of interest here are the 5 MHz blocks labeled G, H, and I and the 10 MHz J block. Through Auction 97 [4], the AWS-3 band was auctioned for commercial mobile broadband usage in the United States. The auction raised \$41B in revenue for the United States Treasury and required federal agencies that were making use of the AWS-3 band to look for other ways to accomplish their missions. To achieve this goal, in the 1755 MHz to 1780 MHz portion of the AWS-3 band, the DoD is using a combination of sharing, compression, and relocation to other bands (including the 2025 MHz to 2110 MHz band).

In 2012, the Commerce Spectrum Management Advisory Committee (CSMAC) was tasked with exploring ways to lower the repurposing costs and/or improve or facilitate industry access to spectrum while protecting specific federal operations from adverse impact, particularly in the AWS-3 band.

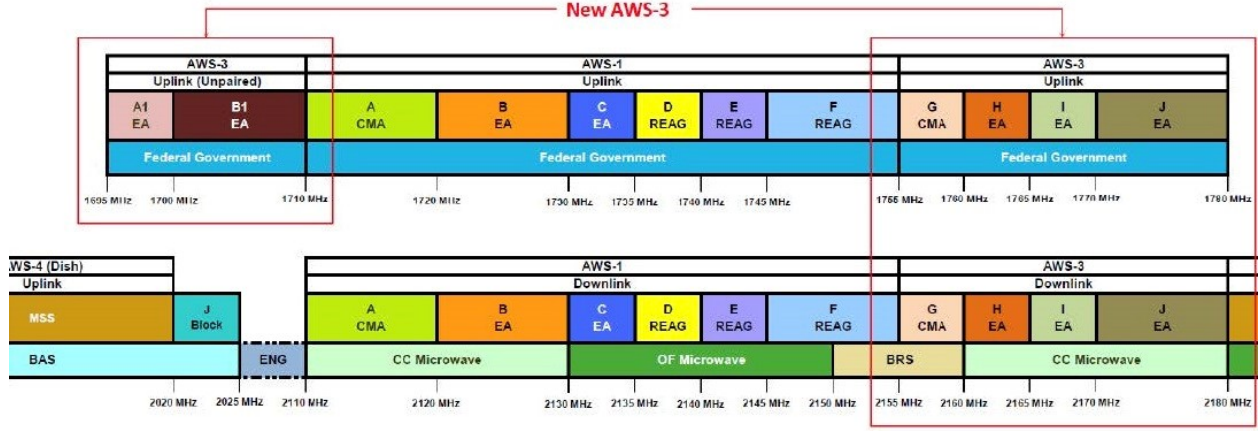


**Figure 1.1:** Description of the AWS-3 Band.

From the AWS-3 auction proceeds, DoD is receiving a spectrum relocation fund (SRF) to implement its approved transition plans. The SRF is also funding evaluation of early entry coordination requests from the auction winners in the AWS-3 band through the DoD early entry portal analysis capability (EEPAC), which is managed by DISA DSO. The portal receives requests from auction winners to enter band(s) before the DoD has transitioned out of the bands. These requests must be considered carefully and impartially to deliver a fair answer. If early entry is granted and there is interference to DoD systems, it would be very costly to the DoD in terms of both financial and mission completeness. If early entry is denied to a commercial carrier for overly conservative reasons, it could be very costly to their business model. To avoid these costs, it is crucial that the findings of the EEPAC are fair and based on a well understood and openly documented methodology.

Towards this end, the DSO is evaluating entry requests by use of an interference equation (1.1) and the effective isotropic radiated power (EIRP) distributions assumed by the CSMAC. To gain further confidence in their calculations, the DSO has asked NASCTN to develop a measurement-based plan for gaining an improved quantitative understanding of LTE uplink emissions. More specifically, NASCTN will investigate how the LTE UE behaves in frequency and power under realistic operating conditions, and how this behavior depends on the network configuration, going beyond the CSMAC analysis with its fixed (and possibly unrealistic) network configurations. The UE antenna pattern measurements presented in this report directly support NASCTN's effort through detailed and realistic antenna pattern measurements.

The interference equation used by the EEPAC <sup>1</sup> [5] is

$$\hat{I}_k = \hat{E}^{(N)} - L_{path} - \hat{L}_{clutter} + G_r(\theta, \phi) - L_{pol} - L_{rec} - R - \Pi, \quad (1.1)$$

<sup>1</sup>We follow the notation of [6]; lower case variables denote numbers in linear units (e.g., mW) while upper case variables use a logarithmic scale (e.g., dBm). Random variables are denoted by a caret. The symbols for the last two terms have been changed from [6] to a single letter for readability.

where

$\widehat{I}_k$  = Interference from the modeled user equipment (UE) in the  $k^{th}$  cell (in dBm)

$\widehat{E}^{(N)}$  = EIRP emitted by  $N$  modeled UEs (in dBm)

$L_{path}$  = path loss between modeled UE and DoD receiver (in dBm)

$\widehat{L}_{clutter}$  = clutter loss between modeled UE and DoD receiver (in dB)

$G_r(\theta, \phi)$  = DoD receiver antenna gain in direction of modeled UE (in dB)

$L_{pol}$  = DoD receiver antenna mismatch loss (in dB)

$L_{rec}$  = DoD system receiver loss (in dB)

$R$  = Frequency-dependent rejection (in dB), known in [6] as  $RFR$

$\Pi$  = Network loading penalty (in dB).

## Chapter 2

# UE Antenna Pattern Measurements and Calculations

### 2.1 Introduction

NASCTN's measurement campaign on "Aggregate LTE: Characterizing UE Emissions" depends on conducting over-the-air (OTA) measurements of LTE UEs uplink emissions in the AWS-3 band. The uplink emissions need to be quantitatively measured, in terms of radiated power. The work is parameterized by LTE network configuration (base station states, co-cell, and adjacent cell activities) and channel (propagation channel impairments). These parameters will be used to assess interference between cellular devices and assets currently near the AWS-3 band. Unless the UE has an isotropic radiation pattern, the measured power will depend on the coupling coefficient of the UE relative to the receiving antenna. For this experiment, we were interested in several aspects of the actual UE radiation pattern.

The first metric of interest was the orientation that provided the maximum coupling in order to provide the geometry that supports the greatest dynamic range in measuring the uplink emissions. A secondary goal became measurement of the depth of nulls in the full three-dimensional pattern of the UE. The null depths indicate the variability in coupling as a function of UE orientation. The third goal, directly realizable from a full three-dimensional pattern, was to determine the actual total radiated power (TRP) from the devices being used in this campaign [7]. The TRP is a spatially averaged metric from the EIRP measured across the radiation pattern. Finally, based on results from the pattern measurements, we present an experiment design for the UE orientation in the Aggregate LTE Project and investigate the associated spatial uncertainties from this choice of orientation.

## 2.2 Experiment Setup

Our first goal was to determine the effect and the introduced uncertainty from the radiation pattern of handheld UEs being used in the LTE aggregate experiment. Specifically, in the experiment we sought to bound the deviation from an isotropic radiation pattern. Spectrum interference calculations often make an assumption of isotropic radiation patterns with expected deviations that should be on the order of  $\pm 2$  dB [8]. Since manufacturers did not readily publish data on their UE emission patterns, we measured patterns of a collection of LTE UEs that span price point, operating system, and dimension. The objective was to assess differences in the radiation pattern based on these factors.

The collection of UEs and their planar dimensions are shown in Table 2.1. The UEs are each given a designation letter. The thickness of the UEs are all comparable and are close to 0.8 cm. Copies of phone A and B were used to assess the repeatability of two different UEs of the same model (but different serial number), hence the quantity parameter is 2. Patterns were only measured on one of each phone, but repeat experiments that will be described later in determining placement uncertainty for the experiment design utilized multiple samples when available.

**Table 2.1:** Collection of LTE UEs used for the study presented here. The letter designator, approximate planar dimensions, and quantity of each UE is shown in the table.

Phone Model	Height (cm)	Width(cm)	Quantity Tested
A	16.0	7.8	2
B	16.0	7.5	2
C	13.0	6.6	1
D	13.8	6.7	1
E	15.8	7.8	1
F	14.2	7.3	1

In order to measure the three-dimensional radiation pattern, we used the NIST Broadband Interoperability Test Facility (NBIT) to provide a far-field environment. Within NBIT, we used the large anechoic environment with a 3 m quiet zone. A schematic of the setup is shown in Figure 2.1. We set up a dual-ridge horn antenna with, nominally, 10.4 dB gain, as calibrated by the manufacturer, as the measurement antenna. It remained in the chamber to measure the UE and the path loss within the chamber. The measurement antenna was mounted on an antenna mast made of dielectric material that provided height and rotational degrees of freedom. We then set up a turntable with a polystyrene foam mount 2.75 m from the measurement antenna as a fixture for the UE.

We measured the UE radiated power (i.e., the uplink power) in a Band 3 allocation with a center frequency of 1775 MHz with a bandwidth of 10 MHz. In order to make sure we were in the far field, we took an antenna aperture for the UE,  $D$ , as the longest dimension of 0.16 m and a lower

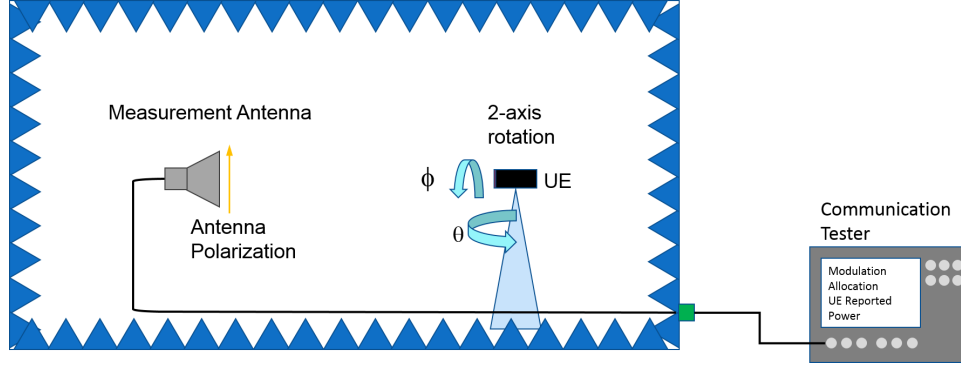


**Figure 2.1:** Schematic representation of the anechoic chamber, measurement antenna, turntable, rotator, and UE. The measurement antenna is shown with vertical polarization. The EIRP is measured using a communication tester (base station emulator).

wavelength limit at 1770 MHz of 0.17 m. Then, the Fraunhofer distance,  $d$ , defined as [9]

$$d = \frac{2D^2}{\lambda}, \quad (2.1)$$

was 0.3 m. Therefore, we were nine times the Fraunhofer limit, effectively in the far-field of the UEs antenna. The aperture of the horn antenna is 0.3 m which puts the measurement at six times the Fraunhofer distance for the measurement antenna, which is still in its far-field as well.

As shown in Figure 2.1, the turntable provided the angular degree of freedom in what we defined as the UE's elevation direction  $\theta$ . We then mounted a small rotational stage on an acrylic plate and used a hook and loop, temporary fastener to affix the acrylic plate's base to the turntable mount. We then attached an acrylic rod to an acrylic block to mount the UE under test. The acrylic rod was attached with a machined adapter to the rotational stage. The UE was attached to the acrylic block using the same hook and loop fastener as before. The small rotational stage provided the UE's azimuth ( $\phi$ ) rotational degree of freedom. An assessment of the effect of the mount on the radiation pattern of the UE is provided in Section 3.1.2. The rotational conventions are taken from the CTIA OTA Test Plan [7]. The small rotational stage used for  $\phi$  was surrounded by radio-frequency (RF) absorber to reduce reflections from the metal of the rotator's motor. At these frequencies, the RF absorber used on the rotation stage is specified to provide 30 dB reduction in reflections. A photograph of the experimental setup is shown in Figure 2.2.

As is shown in Figures 2.1 and 2.2, we used a single antenna connected to a communication tester for both establishing a communication link with the UE and for the measurement of uplink power. A typical setup defined by the CTIA would use two antennas for this measurement. One antenna would establish a communication link with the UE, as we have done here, while the second antenna would be connected to a spectrum analyzer to measure the uplink signal. The technique with two antennas and a spectrum analyzer may provide greater dynamic range than the communication tester is designed to provide [7]. A typical spectrum analyzer may have a noise floor of -130 dBm, where with the communication tester, the noise floor is approximately -90 dBm. However,



**Figure 2.2:** Photograph of the anechoic chamber, measurement antenna, turntable, rotator, and UE. The measurement antenna is shown with vertical polarization. Also, the UE is shown in portrait orientation which is rotated by  $90^\circ$  from the orientation used for the full radiation pattern measurements, and thus the TRP calculation.

we were concerned with the second antenna distorting the radiation pattern through reflections or direct coupling. Therefore, we automated the measurement acquisition software to dynamically adjust the external attenuation setting on the communication tester to allow an increase in dynamic range. This allowed us to measure across a 40 dB dynamic range, down to the noise floor of the communication tester. The increased dynamic range accomplished for the tester was useful for investigating the depths of nulls in the measured radiation patterns without the interference of the second antenna present.

With the experiment setup described above, we measured the radiated power of a UE uplink operating in LTE Band 3, at a center frequency of 1775 MHz. Band 3 was selected as its uplink frequency overlaps with that of the AWS-3 band. We used the communication tester to set the UE to transmit with all physical resource blocks occupied at QPSK modulation and at maximum power. We then measured the average power across the 50 resource blocks with 9 MHz bandwidth, averaged over 20 LTE subframes. This yielded the received power at the input of the communication tester receiver for a given angular configuration of the UE. As described in the rest of this section, by measuring the path loss between the UE and the measurement antenna, we corrected the received power to obtain EIRP, defined as the transmitted power of the UE for that angular configuration. The integrated average of these EIRP measurements over vertical and horizontal polarizations of the measurement antenna will give the TRP for the device and is discussed in Section 2.2.1.

The determination of the path loss in this experiment setup was done by replacing the UE with a reference antenna and measuring the path loss directly. Our reference antenna was a second dual-

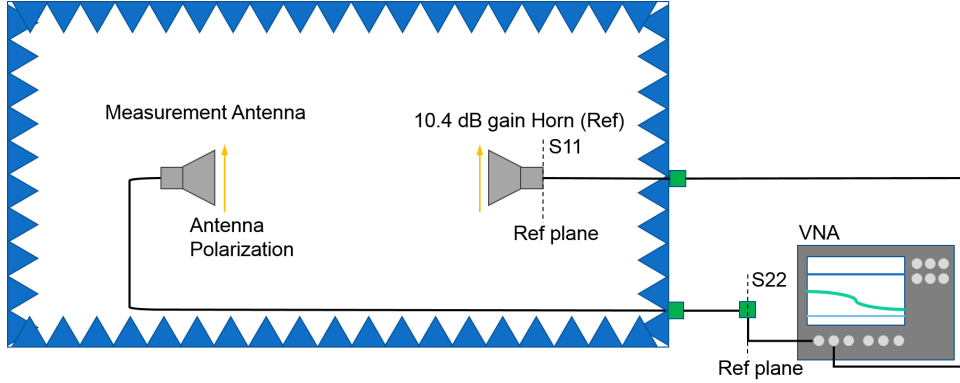


**Figure 2.3:** Schematic of path loss measurement setup.

ridge horn antenna with a nominal gain of 10.4 dB. We used a vector network analyzer (VNA) to estimate how much power was lost between the UE antenna and the input of the communication tester. The path loss setup is shown in Figure 2.3. We calibrated the VNA at the reference planes shown with dashed lines in Figure 2.3. We measured the loss between the reference planes. Since the measurement antenna is present for both the path loss measurement and the EIRP measurements, we can ignore the gain of the measurement antenna and the loss in the connecting cable. However, we must account for the gain of the reference antenna. If the UE power in the uplink channel measured at the communication tester receiver is called  $P_m$ , the reference antenna has gain  $G$ , and the measured path loss is  $L_{path}$ , then the EIRP at the UE antenna, in Watts (W), is

$$EIRP = \frac{P_m G}{L_{path}}. \quad (2.2)$$

We conducted four measurements in order to estimate the path loss of this experiment setup with changes in the setup to simulate potential systematic errors. We first copolarized and aligned the reference antenna to the measurement antenna coarsely by eye, then optimized by maximizing the magnitude of  $S_{21}$ . We next moved the reference antenna approximately 5 cm further away from the measurement antenna to account for uncertainty in the location of the phase center of the reference antenna based on its physical dimensions. For a third measurement, we moved the reference antenna 5 cm vertically up. Finally, the measurement and reference antennas were rotated  $90^\circ$ , height adjusted to align the antennas, and measured again. This simulated the changes for the orthogonal polarization measurements of the patterns. For each of the four measurements, we calculate

$$L_{path} = \frac{\langle |S_{21}| \rangle_f^2}{1 - |\langle S_{11} \rangle_f|^2}, \quad (2.3)$$

where  $L_{path}$  is the unit-less range loss,  $S_{21}$  is the forward transmission coefficient,  $S_{11}$  is the reflection coefficient measured by port 1 of the VNA at the reference plane of the cable connection

at the reference antenna, and the angle brackets represent a frequency average over the 10 MHz bandwidth centered at  $f = 1775$  MHz. At each of the four positions described, 20 measurements of  $L_{path}$  were performed. The the average path loss in dB is calculated as,

$$L_{path}(\text{dB}) = 10\log_{10}(\overline{L_{path}}), \quad (2.4)$$

where  $\overline{L_{path}}$  is the linear mean of the 80 measurements (20 repeats at four configurations). The uncertainty, in dB, is then given by

$$\sigma L_{path}(\text{dB}) = 10\log_{10}\left(\frac{\overline{L_{path}} + \sigma L_{path}}{\overline{L_{path}}}\right), \quad (2.5)$$

where  $\sigma L_{path}$  is the standard deviation of the mean between the means of the four different path loss measurements. The path loss was estimated to be 33.8 dB before accounting for the reference antenna gain with a relative uncertainty of 1.2 dB. The standard deviation of the mean of the repeats for a given configuration was neglected in this calculation since it ranged between 0.001 and 0.01 dB.

The gain of the reference antenna was taken from the manufacturer's specification sheet. The gain measurements from the manufacturer included a relative uncertainty of 0.75 dB. The gain, including the efficiency, was measured by the manufacturer at 1750 MHz and spaced every 250 MHz. We linearly interpolated the data to estimate a gain of 10.4 dBi at 1775 MHz with only 0.05 dB variation across the 10 MHz bandwidth. However, since linearity in the gain as a function of frequency can not be assumed, we take the difference of the gain at the next measured frequency points as an overestimate of uncertainty due to the interpolation and attribute 0.5 dB relative uncertainty to this procedure. We will treat the manufacturer's measurement uncertainty and the interpolation uncertainty as independent and sum them in quadrature. Since these quantities are in logarithmic units, we must first convert them to linear before combining them. For a general variable,  $h$ , with an uncertainty given in dB,  $\sigma h(\text{dB})$ , we can determine the relative uncertainty in linear units according to the relation,

$$\frac{\sigma h}{h} = 10^{\frac{\sigma h(\text{dB})}{10}} - 1. \quad (2.6)$$

Thus, converting to linear units according to eqn. 2.6, adding them in quadrature, and converting back to dB yields a combined relative uncertainty of 0.9 dB.

The uncertainty, in watts, from eqn. 2.2 may then be given by

$$\sigma EIRP = EIRP \sqrt{\left(\frac{\sigma P_m}{P_m}\right)^2 + \left(\frac{\sigma G}{G}\right)^2 + \left(\frac{\sigma L_{path}}{L_{path}}\right)^2}. \quad (2.7)$$

The terms under the radical are the relative uncertainties in linear units which are derived from the

logarithmic quantities from eqn. 2.6.

We previously estimated the gain uncertainty  $\sigma G$  as 0.9 dB or 0.225 as a relative ratio and the range loss uncertainty  $\sigma L_{path}$  as 1.2 dB. The measured uplink power over 20 subframes had a very low uncertainty as calculated by the communication tester. The variability was on a timescale in excess of 20 subframes. However, from repeat measurements at various power levels, the spread in values of the 20 subframe averages was 0.5 dB higher than the reported uncertainty. This estimate comes from repeat measurements of the 20 subframes for the low power levels in the radiation pattern. This is an overestimate of  $\sigma P_m$  for locations with good connection strength, and could be refined if needed in the future. The total uncertainty ascribed to the EIRP measurements taken here is 1.5 dB from eqn.2.7.

## 2.2.1 Total Radiated Power

A useful metric to check the validity of the UEs performance is the total radiated power (TRP). Although we looked at patterns with a constant angular step of  $5^\circ$  in each rotational dimension, the industry standard calls for  $15^\circ$  steps [7]. The TRP calculation in [7] is defined as

$$TRP = \frac{\pi}{2NM} \sum_{i=1}^{N-1} \sum_{j=0}^{M-1} [EIRP_H(\theta_i, \phi_j) + EIRP_V(\theta_i, \phi_j)] \sin(\theta_i), \quad (2.8)$$

where  $N = 11$  is the number of  $\theta$  positions for  $15^\circ$  steps,  $M = 24$  is the number of  $\phi$  positions for  $15^\circ$  steps,  $EIRP_H$  is the EIRP with the measurement antenna in horizontal polarization and  $EIRP_V$  is in vertical polarization, and  $\theta$  and  $\phi$  are defined in Figure 3.9. Using (2.8), and taking a sparser,  $15^\circ$  sampling the collected data, the results for the phones in this study are shown in Table 2.2. The uncertainty is taken from the individual measurements of EIRP.

**Table 2.2:** Calculation of TRP From Three-Dimensional Radiation Patterns ( $15^\circ$  steps)

Phone	TRP (dBm)	Unc (dB)
A	19.6	1.5
B	21.6	1.5
C	17.5	1.5
D	17.3	1.5
E	18.7	1.5
F	16.0	1.5

## 2.2.2 Uncertainties due to UE Orientation

The angular control fixture we built for the large anechoic chamber provides a good opportunity to look into repeatability between phone models and, additionally, different phones of the same model. This will give an indication as to what we can expect from the subsequent aggregate emissions experiments. Another source of uncertainty assessed was the effect of having the power cord of the UE attached during the experiment. The patterns discussed up to this point have been with the UE unplugged, as is the typical use case. However, for the LTE aggregate experiment, the UE will have the power cable attached during the experiment so that diagnostic monitoring software can be used to collect data from the UEs chipset during the experiments. Therefore, we also assess the uncertainty of having the cable attached.

We used two copies of phones A and B. Initially, we were searching for the orientation of the UE that would yield the maximum radiated power to the measurement antenna in order to maximize the experiment's dynamic range. However, the power cable complicates this. As can be seen in Figure 2.4A, the UE without a power cable shows small deviations in output power for small changes in angle. The deviations are smaller than the EIRP measurement uncertainty over a  $10^\circ$  change in  $\theta$  and  $\phi$  and are shown in Figure 2.5. Figure 2.5 shows repeat measurements using two pairs of different phones (four phones total), with the top of the phones copolarized with the measurement antenna. Also included in the repeatability are the orientations  $5^\circ$  away from the peak orientation. Thus, there are two effects captured in the histogram, angular deviations up to  $5^\circ$ , and phone variability. Here we see a peaked distribution of results with a relative uncertainty of 0.5 dB calculated as the standard deviation of the distribution. On the other hand, inclusion of the power cable in the phone as is seen in Figure 2.4B removes the angular stability and will make repeatable measurements very difficult.

Including the power cord in the UE is vital for this experiment in order to extract information from the UE chipset during measurements. Therefore, we determined that the optimal technique to mitigate angular instability is to orient the cable orthogonal to the polarization of the measurement antenna at all times. Another technique for mitigation of cable effects is to add electromagnetic interference chokes to the cable. We did not investigate this solution, but would add this to future measurement campaigns. From the patterns, we have seen that we can achieve close to the maximum output power by co-polarizing the top of the phone with the measurement antenna. This will allow the cable to remain orthogonal to the measurement antenna during the aggregate LTE measurement campaign. To assess the uncertainty contribution and offset we can expect from including the cable in the measurement, we performed repeat measurements of phones A and B, with the cable present. A repeat consisted of removing the phone from the test fixture, unplugging it, then replugging with the cable in a new orientation and placing back in the measurement fixture. These repeats were done for two copies, or samples, of phone A and two copies of phone B. The results are shown in Figure 2.6. The repeatability is much worse and does not show a normally distributed pattern. In this experiment, the cable was left unfixed in order to observe the full range of expected variation. Here, with the approximation of a normal distribution, the relative uncer-

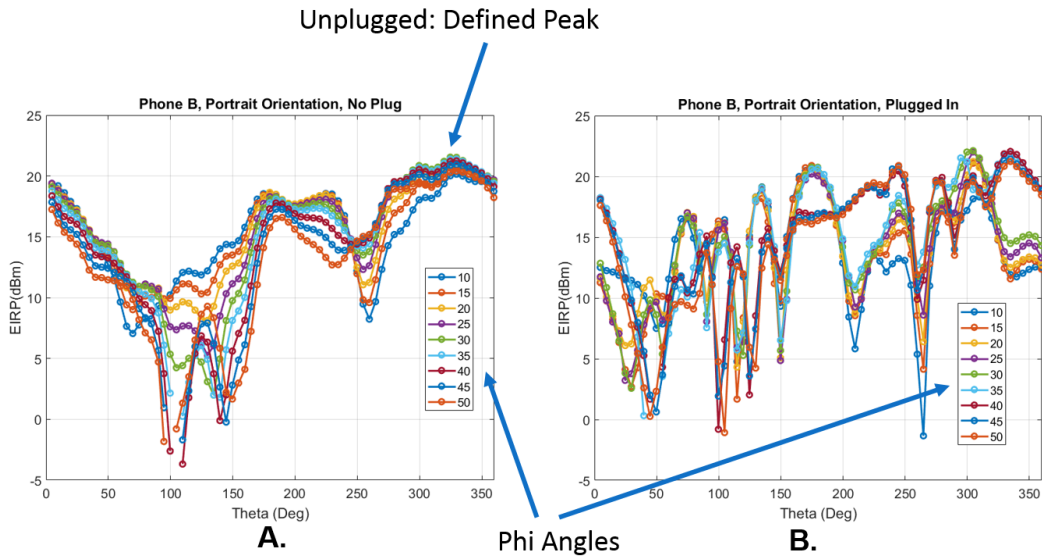


**Figure 2.4:** Measured EIRP versus  $\theta$  at several orientations of  $\phi$  with A.) no power cable present, and B.) with the charging cable plugged in to line power. Phone B, sample 1 is shown in the plots.

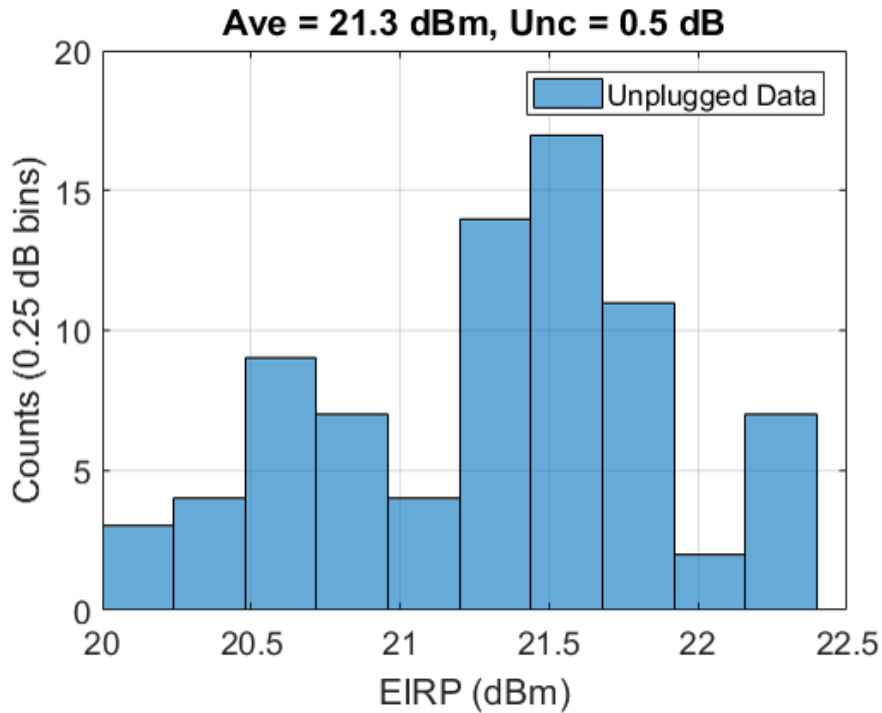


**Figure 2.5:** Histogram of EIRP from 20 repeat measurements with phone A and B (2 units each) with no charging cable present using 0.25 dB bins. The histogram includes angles  $5^\circ$  away, in both measurement angles, from alignment and co-polarization of the top of the UE with the vertically polarized measurement antenna.

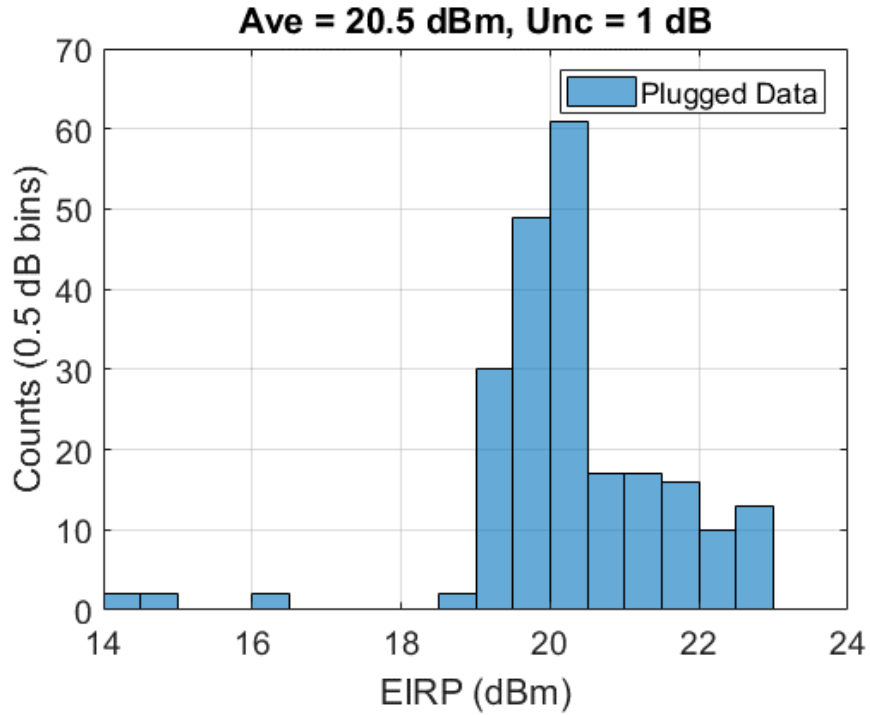


**Figure 2.6:** Histogram of EIRP from repeat measurements of phones A and B with the power cable present using 0.25 dB bins. The histogram includes intentional measurement misalignments; 5 degree off axis alignment in geometry and polarization with respect to the vertically polarized measurement antenna.

tainty is measured to be 1 dB. The offset in measured average power is within the measurement uncertainty, but lower by less than 1 dB.

# Chapter 3

## Measurement Results

We performed full three-dimensional pattern measurements of several UEs utilizing a rotating fixture as shown in Fig. 2.1. In this chapter, we discuss characterization of the three-dimensional fixture by comparison to a more transparent polystyrene fixture with only one rotational degree of freedom. We then show results of the comparison and finally present the full patterns measured on the UEs.

### 3.1 Fixture

In order to understand the perturbations caused by the rotating fixture, we first compared results to a minimally invasive mount made of polystyrene foam. We present measurements and analysis of the foam and bi-axially rotating fixtures.

#### 3.1.1 Polystyrene Mount

Before performing measurements with the  $\phi$  rotation stage, we first mounted the UE under test in a 1 inch thick piece of polystyrene foam. This simple mount avoids the shadowing effects and reflection(s) that may be present with the additional motor mount and absorber. A slit in the polystyrene mount just large enough for the depth of the UE was carved out and the UE held in both vertical (portrait) and horizontal (landscape) orientation on top of the turntable. Thus, the foam formed a base on top of the  $\theta$  rotation turntable with only a small portion of the phone held in it. The goal was two-fold. First, to determine as clean of a pattern, in two dimensions, as possible before using the full bi-axial rotational setup. Second, it allowed a quick electrical alignment to determine where in the UE the antenna elements may be and provide some intuitive expectations for the antenna behavior. The data using the foam mount were collected only for phones A,B, and

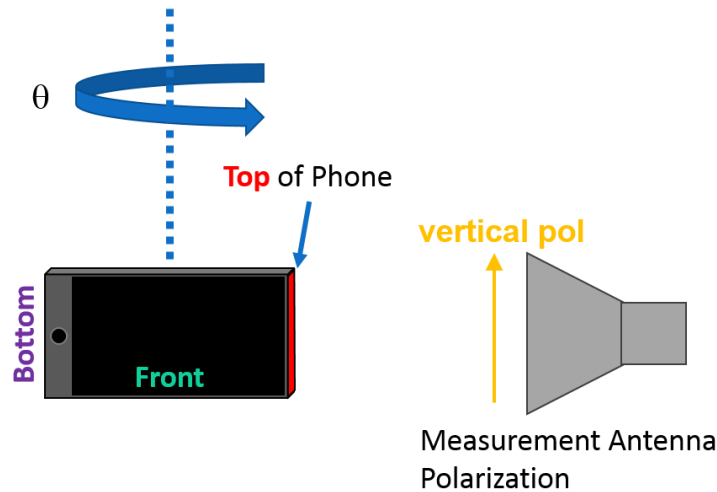


**Figure 3.1:** Schematic showing the orientation of the landscape-oriented UE relative to the vertically polarized measurement antenna for the  $\theta = 0^\circ$  position. The turntable rotation,  $\theta$ , is shown by the wrap-around arrow.

C.

Figure 3.1 shows the orientation of the UE relative to the measurement antenna. Also indicated is the direction of rotation of the turntable,  $\theta$ . Figure 3.2 shows the two-dimensional pattern of this elevation rotation, or “cut.” The angles for which the top and bottom of the UE are closest to the measurement antenna are shown. There are a few interesting features to note. To first order, in this analysis it is helpful to assume a dipole-like linearly polarized radiation pattern aligned with the top and bottom of the phone. Of course, they are not ideal dipoles - for the generation of phone tested in this report, the antennas are typically inverted F antennas - but the dipole approximation is helpful for understanding the pattern [10]. The tops of the phones are co-polarized with the measurement antenna for the full  $\theta$  rotation. All the phones behave similarly when the end that presumably contains the antenna is closest to the measurement antenna. Phone A has an asymmetry not seen in any other phone, however, it is repeatable for both phones of this type.

The next measurement was performed with the UE in landscape orientation as above, but with the measurement antenna horizontally polarized, as shown schematically in Figure 3.3. If the antenna were just a dipole in the top or bottom of the UE, then this orientation would show a very large extinction ratio due to complete cross polarization. As seen in Figure 3.4, all three phones tested did show a large extinction ratio due to cross-polarization. However, they all showed significantly more radiated power with the front and back of the phone exposed to the horizontally polarized antenna than would be expected in a cross-polarized state. The measured power is reduced by 10 dB from the peaks of Figure 3.2, but are not completely cross polarized.

The deviation from dipole behavior can also be seen by orienting the UE in the portrait orientation with the polystyrene mount. A schematic of this scenario is shown in Figure 3.5. Both measure-

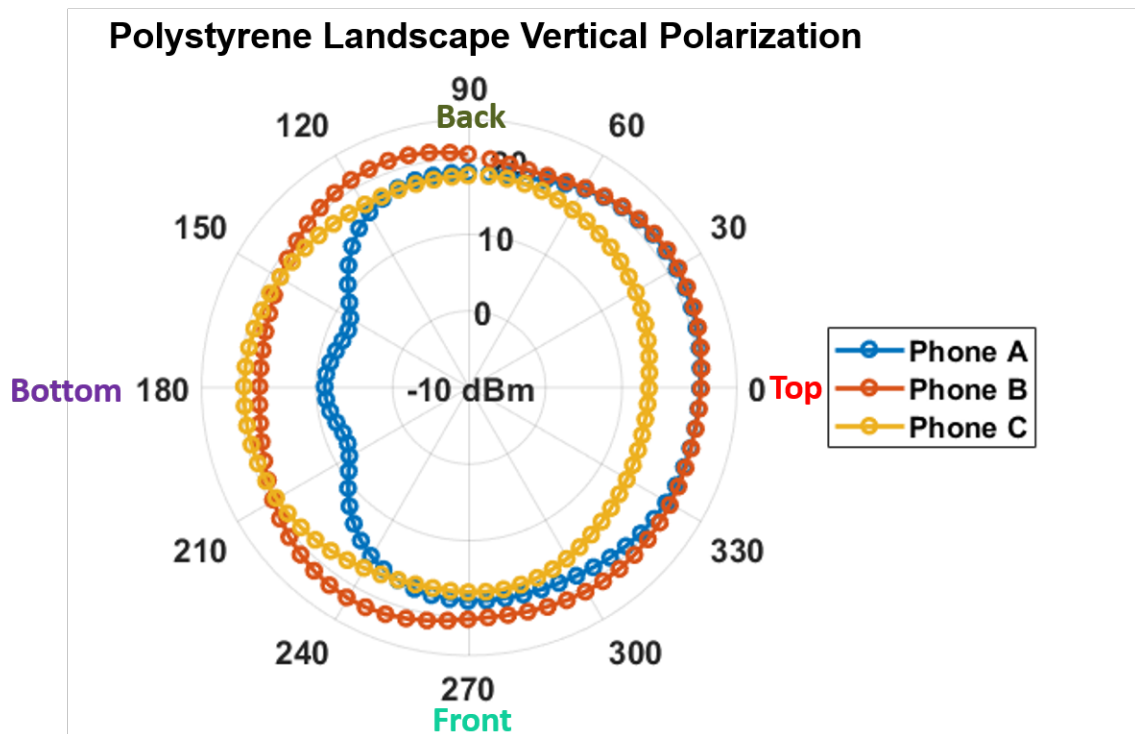


**Figure 3.2:** Antenna pattern from Phones A, B, and C (shown in blue, red, and yellow, respectively). The UE was held in the landscape position with the measurement antenna vertically polarized.

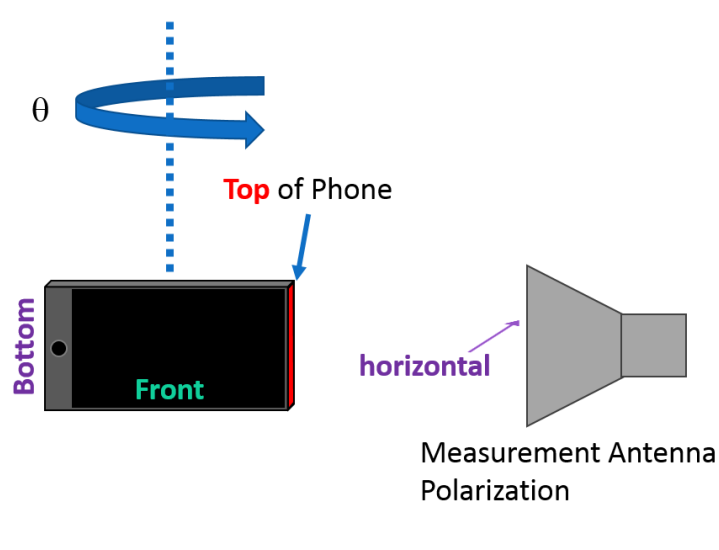


**Figure 3.3:** Sketch showing the orientation of the landscape-oriented UE relative to the horizontally polarized measurement antenna for the  $\theta = 0^\circ$  position. The turntable rotation,  $\theta$  is shown with the wrap-around arrow.

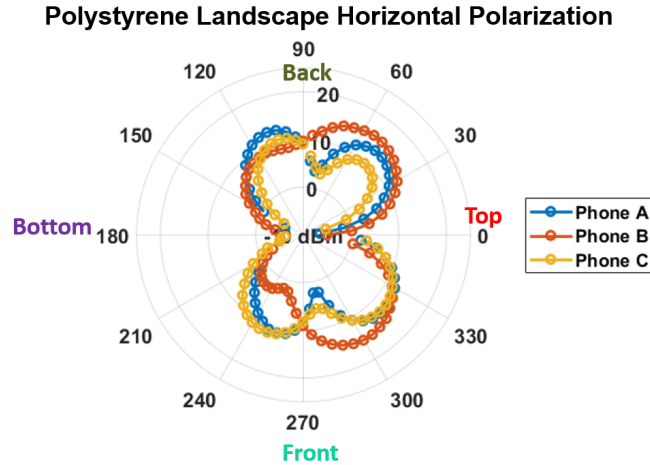


**Figure 3.4:** Radiation patterns from UE’s A, B, and C (shown in blue, red, and yellow, respectively). The UE was held in the landscape position with the measurement antenna horizontally polarized. In the approximation that the antenna is at the top of the phone, this orientation should provide complete cross polarization.

ment antenna polarizations are represented in the figure. The measurement results are shown in Figure 3.6. Figure 3.6A shows the pattern with the measurement antenna in vertical polarization, and Figure 3.6B is the horizontal measurement antenna polarization result. If the antenna were truly just a dipole antenna in the top or bottom of the phone, there would be no received signal in the vertical polarization of the measurement antenna. There is a component of the antenna radiation pattern that is co-polarized with the vertical polarization of the measurement antenna even in the portrait orientation of the UE. The horizontally polarized measurement antenna picks up more radiated power, at the peaks, than when it is vertically polarized, especially with the front or back of the UE exposed to the antenna. It is interesting to note that the nulls in the UE pattern detected for the vertical polarization of the measurement antenna occur with the front and back of the UE exposed directly to the measurement antenna, which are the inverse of the horizontal polarization measurement antenna. The horizontally polarized result matches the idealization of a dipole approximation in the top or bottom of the UE.

### 3.1.2 Effect of Three-Dimensional Rotation Fixture

After initial measurements with the foam mount, we built the full  $4\pi$  rotation setup shown in Figure 2.2. Before measuring the full pattern, we needed an understanding of the nonidealities contributed by the motor mounts, absorber, and acrylic fixtures. With the UE in portrait orientation, with varying tilt angles, the two-dimensional cuts in the  $\theta$  direction were measured. The UE was mounted on one side of the acrylic block, starting with the screen (front) of the UE oriented away from the measurement antenna with the block between the UE and the antenna at  $\theta = 0^\circ$ , as depicted in Figure 3.7A. These are the curves in Figure 3.7C-3.7E labeled “away.” Reproducibility

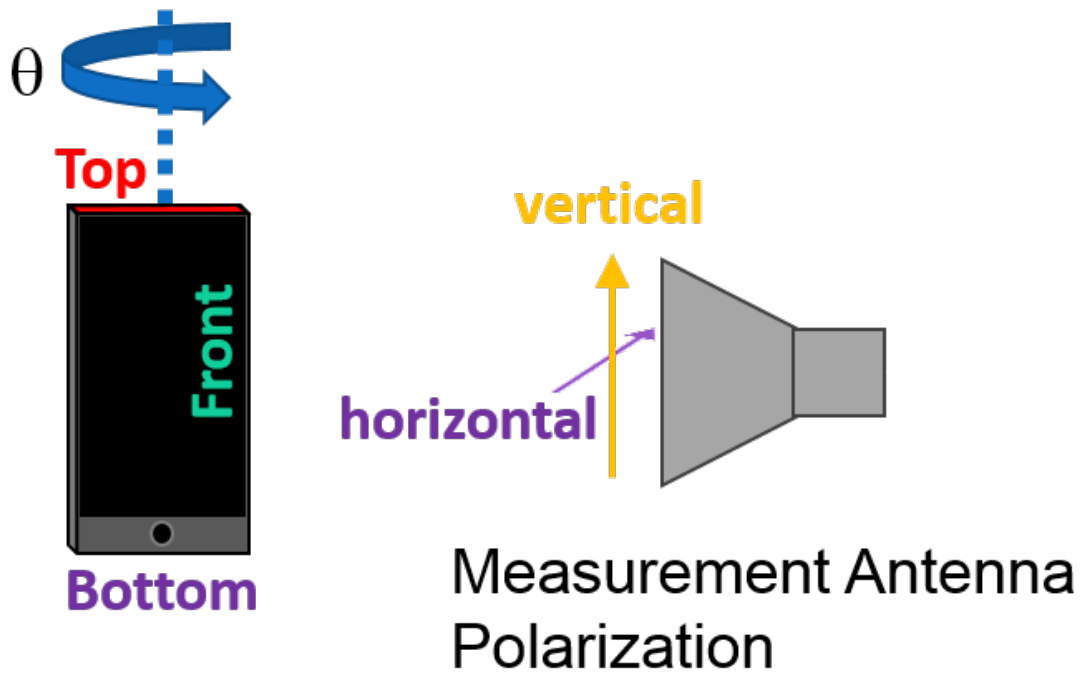


**Figure 3.5:** Schematic showing the orientation of the portrait-oriented UE relative to both vertically and horizontally polarized measurement antenna for the  $\theta = 0^\circ$  position. Again, the turntable rotation,  $\theta$ , is shown by the wrap-around arrow.

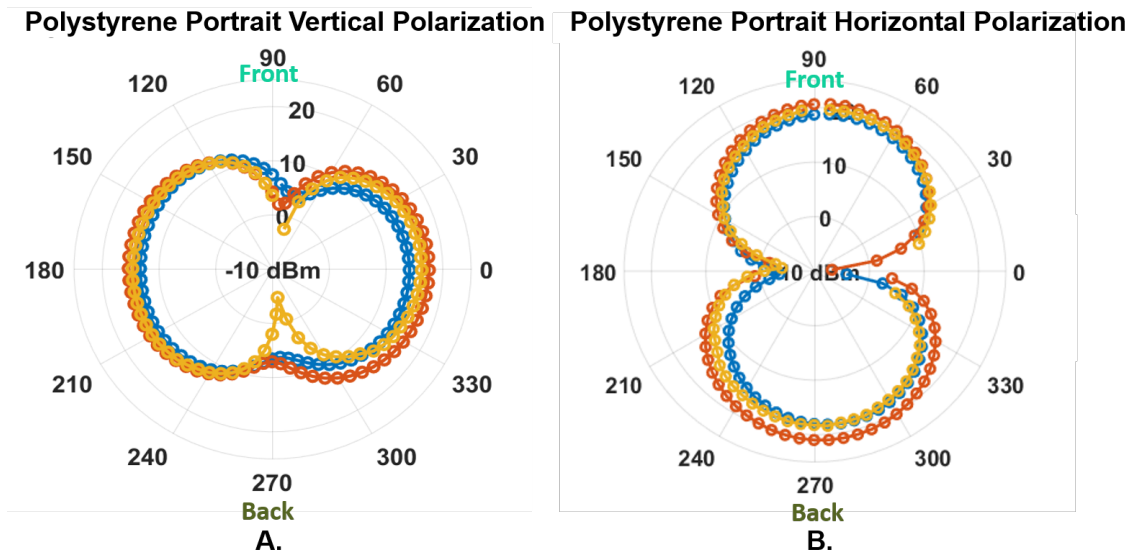


**Figure 3.6:** Radiation patterns from UEs A,B, and C (shown in blue, red, and yellow, respectively). The UE was held in the portrait position in the foam mount. The measurement antenna was polarized, (A.) vertically, (B.) horizontally.

was checked by removing the UE and placing it back on the acrylic block in the “away” orientation. The result of this measurement is labeled in the same plots as “repeat”. The reproducibility was very good, less than 1 dB variation between repeats. Then, the UE was mounted on the opposite side of the acrylic block in the “face” orientation, meaning initially, at  $\theta = 0^\circ$ , the block is behind the UE and nothing is between the UE and the measurement antenna. The  $\theta$  scan was performed with  $15^\circ$  step size and compared to the “away” data. The “face” data were translated in order to match angles for comparison so that the overlapping data represent the same orientation at each point.

Three sets of data are shown for phone A, sample 1 with the top of the phone tilted away from the measurement antenna at  $\theta = 0^\circ$  (represented by an elevation of  $-15^\circ$  and  $-30^\circ$  in Figures 3.7C and 3.7D) and tilted toward the measurement antenna as represented by the positive elevation in Figure 3.7E. The acrylic block has an effect on the measurement with a maximum of 1-2 dB, which represent a maximum addition of 0.5 dB as compared to the measurement uncertainty of 1.5 dB. However, it should be noted that the block does not alter the pattern measurement at most angles since the electrical alignment data showed the UE pattern to peak at the “top” or “bottom” of the UE geometry. These results indicate that even with attenuation that may be caused by using the acrylic mounting block, at the magnitude scales of interest in this experiment, the acrylic has little effect.

Another experiment to assess the effects of the full bi-axial measurement fixture was to mount the UE in this setup in the landscape orientation, orient the measurement antenna with vertical polarization, and compare this to a similar measurement in the polystyrene mount. The orientation of the phone in the motorized setup is shown in Figure 3.8. This is the orientation that matches the test plan published by CTIA [7]. The results of the comparison are shown in Figure 3.9, which shows the measured EIRP as a function of  $\theta$ . The data for the polystyrene mount are taken from the measurement that yielded those data in Figure 3.2 for phone A, sample 1. The effect of the motorized mount is not significant at most angles. However, as would be expected, signal blockage occurs at  $180^\circ$  since this is where the absorber and motor are between the UE and the measurement antenna. Angles near this  $180^\circ$  point will suffer up to 5 dB attenuation. These points are not considered in TRP calculations. If this orientation becomes relevant for an experiment, the loss due to mounting will need to be measured and corrected.

## 3.2 Full Three-Dimensional Patterns

Given the angles defined in Figure 3.8, we now look at the full radiation pattern from the cell phones defined in Table 2.1. To start with, we show the results from phone B since it’s pattern is the most isotropic and easier to interpret. Figure 3.10 shows the pattern measured for phone B with the measurement antenna in vertical polarization. For calculating TRP according to [7], only  $15^\circ$  steps were necessary, but we were also interested in measuring the depth of nulls present in the

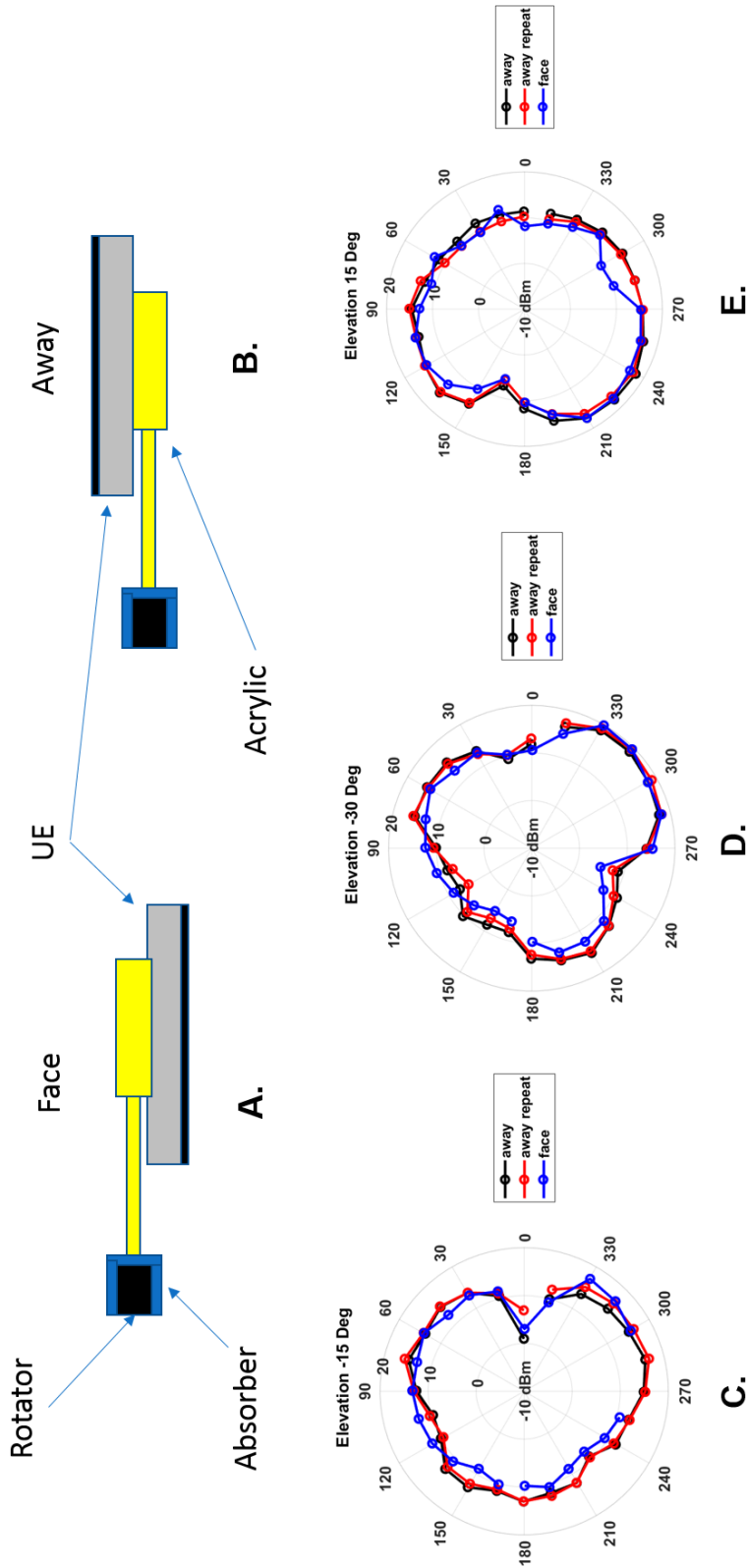


**Figure 3.7:** A and B show the mounting of the UE on the acrylic block with temporary fastener in “Face” and “Away” orientations. The “Face” orientation has the mounting block between the UE and the measurement antenna at  $\theta = 0^\circ$  orientation of the turntable, while the “Away” orientation has the phone’s screen (shown in black) in direct line of sight with the measurement antenna. C shows three measurements, all with the phone tilted  $\phi = -15^\circ$  with the screen downward and the top higher. The black curve is a measurement of the “Away” configuration, while the red curve is a check of reproducibility. The blue curve is the “Face” configuration. D and E have similar results for  $\phi = 30^\circ$  tilt with the screen downward (D) and  $\phi = 15^\circ$  tilt with screen pointing upward. The conclusions from these results are the excellent reproducibility with the  $4\pi$  setup and the overlap of results even with possible blockage from the acrylic mounting block.

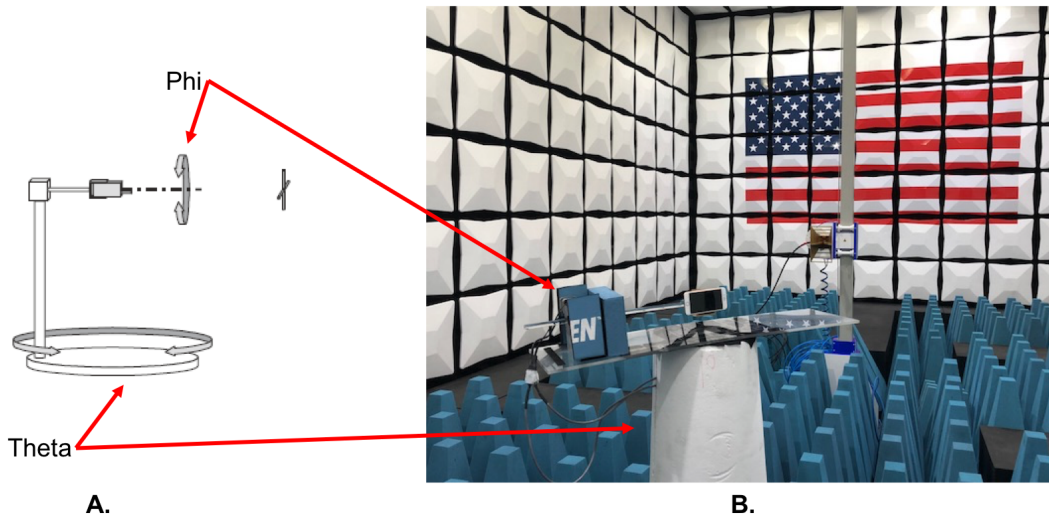


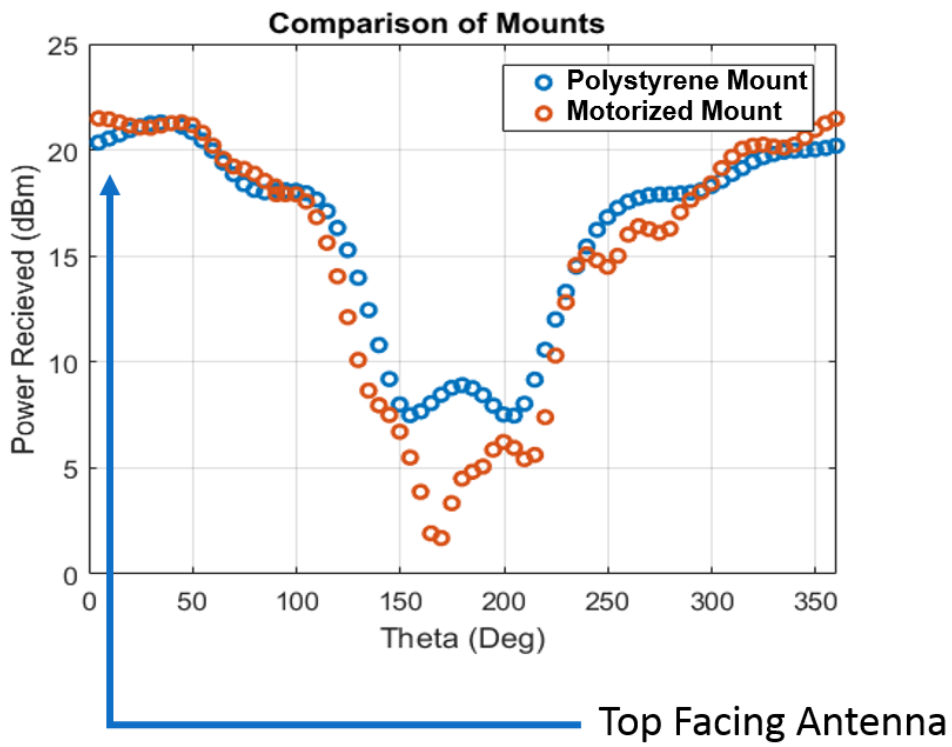
**Figure 3.8:** (A.) Sketch of UE in a motorized fixture with  $\theta$  and  $\phi$  as defined by the CTIA OTA test plan [7]. (B.) The fixture we built to correspond to the schematic in A. The corresponding rotating elements are shown with red arrows.

pattern so the measurement were performed with  $5^\circ$  angular steps.

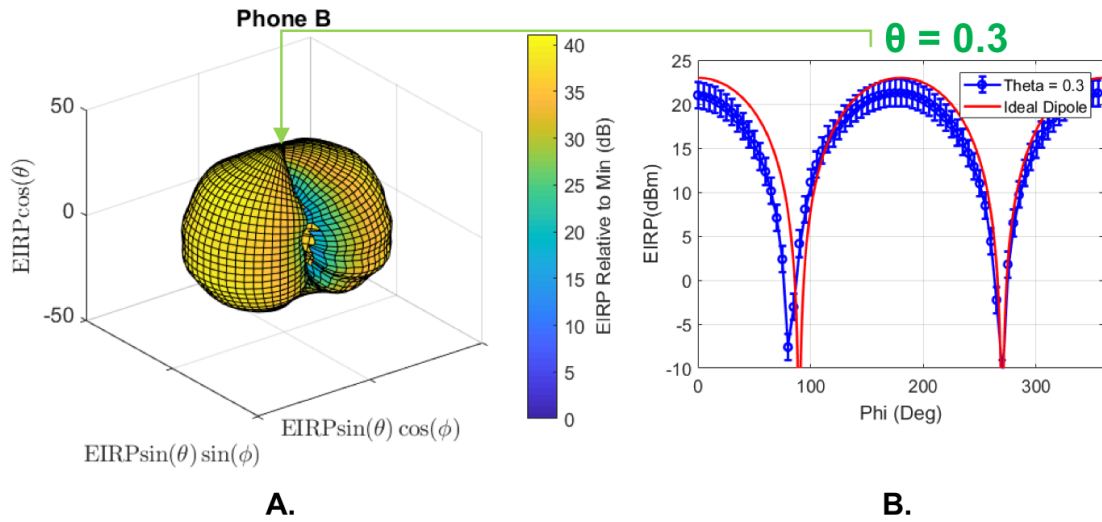
The three-dimensional pattern shown in Figure 3.10A shows the  $\phi$  angles as horizontal cuts, with the equator representing the cut at  $\theta = 90^\circ$ . The color scale shows relative dB power where the minimum of the pattern is set to 0 dB. The first salient feature of this pattern is the deep, 40 dB, null present with cross polarization of the top of the phone with the measurement antenna. Figure 3.10B shows the  $\phi$  cut at  $\theta = 0.3^\circ$ , corresponding to a top view of the three-dimensional plot and indicated by the arrow. Figure 3.10B shows the top of the UE copolarized with the measurement antenna at  $\phi = 0^\circ$ . The vertical axis is the measured EIRP in dBm. Also plotted is the effect of two dipoles being rotated relative to one another to yield  $\cos^2$  behavior, normalized to a maximum power of 23 dBm. The behavior of the UE in landscape rotated around the  $\phi$  axis is well approximated by a dipole antenna pattern.

Figure 3.11 shows the same three-dimensional data for phone B with a horizontal cut taken at  $\theta = 90.3^\circ$  in Figure 3.11B. The ideal dipole behavior is also plotted. With the assumption of a dipole antenna in the top of the phone, we expect only a slight change in behavior since the dipole field will still follow  $\cos^2$  behavior rotating toward the antenna rather than parallel to it. Similar behavior is seen in this orientation, although the maximum radiated power is reduced more than would be expected for the slightly increased distance of top of the phone, perhaps due to shielding effects of the body of the phone.

Next, we look at a vertical cut in Figure 3.12. The two-dimensional cut shown in Figure 3.12B is taken with  $\phi = 0^\circ$ . The top of the phone is copolarized with the vertically polarized measurement antenna. As  $\theta$  is traversed, the top of the phone moves further from the measurement antenna



**Figure 3.9:** Plots of the EIRP versus the turntable angle,  $\theta$ , for the measurement antenna vertically polarized and the UE mounted in landscape orientation in the polystyrene mount (blue) and the  $4\pi$  fixture (red). The label and arrow indicate that at  $\theta = 0^\circ$ , the top of phone A is nearest the measurement antenna and is co-polarized.



**Figure 3.10:** (A.) The three-dimensional antenna pattern of phone B with the measurement antenna vertically polarized. The  $\theta$  direction is in the vertical plane of the figure, while the  $\phi$  direction is the horizontal plane. The measured EIRP is the color scale which is set to a relative scale so that the minimum measured is at to 0 dB. (B.) The horizontal, or  $\phi$  cut taken at the top of the three-dimensional pattern at  $\theta = 0.3^\circ$  as indicated by the arrow. The plot shows the actual measured EIRP in dBm versus the angle  $\phi$ .

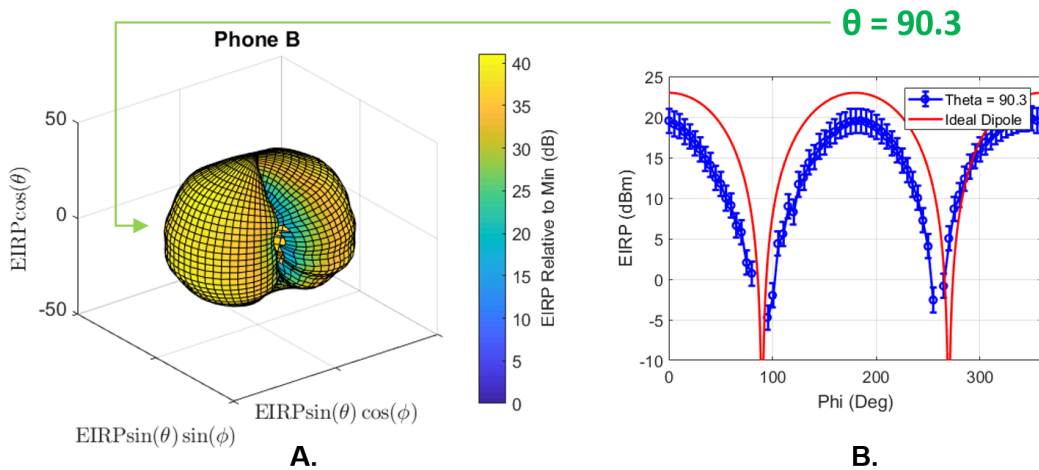


**Figure 3.11:** (A.) The three-dimensional antenna pattern of phone B with the measurement antenna vertically polarized, as shown in figure 3.10. The  $\theta$  direction is in the vertical plane of the figure, while the  $\phi$  direction is the horizontal plane. The measured EIRP is the color scale which is set to a relative scale so that the minimum measured is at to 0 dB. (B.) The horizontal, or  $\phi$  cut taken at the equator of the three-dimensional pattern at  $\theta = 90^\circ$  as indicated by the arrow. The plot shows the actual measured EIRP in dBm versus the angle  $\phi$ .

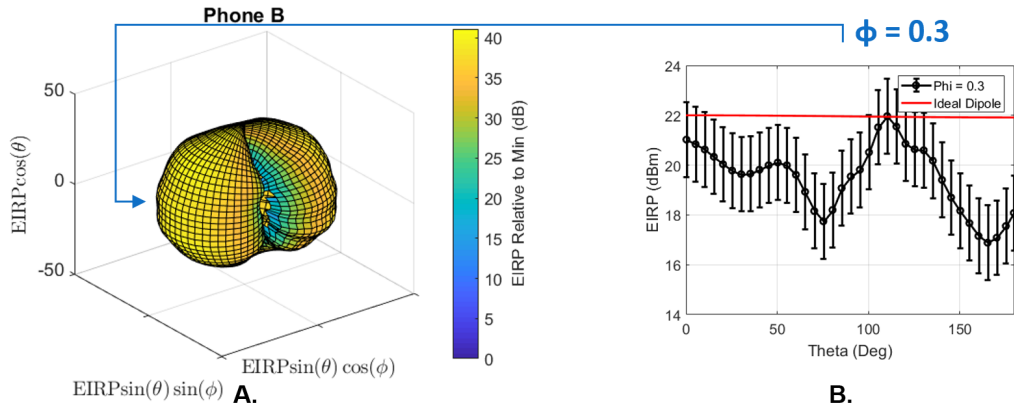


**Figure 3.12: ]**

(A.) The three-dimensional antenna pattern of UE B with the measurement antenna vertically polarized, as shown in figure 3.10. The  $\theta$  direction is in the vertical plane of the figure, while the  $\phi$  direction is the horizontal plane. The measured EIRP is the color scale which is set to a relative scale so that the minimum measured is at to 0 dB. (B.) The vertical, or  $\theta$ , cut taken with the top of the phone copolarized with the measurement antenna. The plot shows the actual measured EIRP in dBm versus the angle  $\theta$ .

maintaining the landscape orientation as it rotates. Again, the relative radiated powers are shown in the three-dimensional pattern in Figure 3.12A, and the measured EIRP corrected for path-loss and reference antenna gain is shown in Figure 3.12B. The expected response from a dipole in the top of the UE is shown as well. The EIRP as a function of  $\theta$  is relatively flat compared to the cuts in Figures 3.10 and 3.11. However, the fluctuation in EIRP is greater than what would be expected for a dipole antenna located where the top of the phone is. It was also surprising to see a peak just above  $\theta = 100^\circ$ , where the expected peak was at  $\theta = 0^\circ$ . The difference in peak power is less than the error bars so further investigation to reduce these errors would be required to verify the alternate peak.

Finally, we look at the radiation pattern from the UE with a horizontally polarized measurement antenna. Again, as the first example we look at phone B, but will compare the patterns of all the phones in this study in Figures 3.17 and 3.18. In Figure 3.13A, the three-dimensional pattern is shown for this polarization and the horizontal cut at  $\theta = 0^\circ$  is shown in Figure 3.13B. This matches the dipole behavior seen Figure 3.10 with a  $90^\circ$  shift in the peaks and nulls, as expected. At  $\theta = 90^\circ$ , we would expect, from the approximation of a dipole in the top of the UE, that the UE would be completely cross polarized to the horizontal polarization of the measurement antenna. However, the EIRP is reduced by 5-10 dB, except for a 23 dB null with the front of the phone facing the antenna. Figures 3.15B and 3.16B show the  $\theta$  cuts of the three-dimensional patterns at two different azimuth angles. The waist seen in the pattern at  $\theta = 90^\circ$  does not represent a global minimum of the pattern which is actually 30 dB below the peak output EIRP. The  $\phi = 90^\circ$  cut shows the co-polarized orientation  $\theta = 0^\circ$ , with an EIRP of close to 23 dBm. However, a deep null

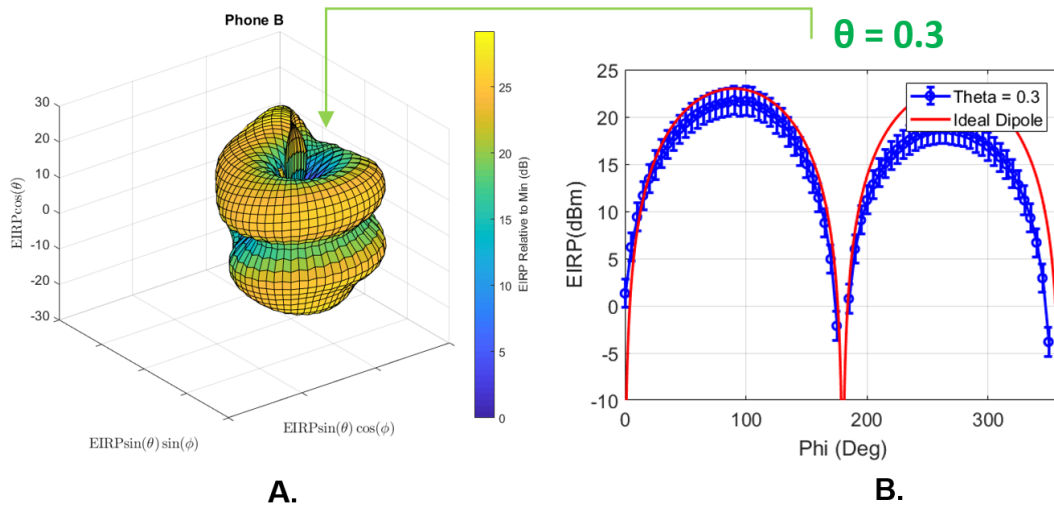


**Figure 3.13:** (A.) The three-dimensional antenna pattern of phone B with the measurement antenna horizontally polarized. The  $\theta$  direction is in the vertical plane of the figure, while the  $\phi$  direction is the horizontal plane. The measured EIRP is the color scale which is set to a relative scale so that the minimum measured is at to 0 dB. (B.) The horizontal or  $\phi$ , cut taken at  $\theta = 0.3^\circ$  which is at the top of the three-dimensional pattern, as indicated by the arrow. At  $\phi = 0^\circ$ , the top of the phone is cross polarized with the measurement antenna. Also plotted, in red, is the expected ideal dipole-dipole behavior.

is never achieved with a 15 dB drop seen with this cut. Apparently, the UE antenna is optimized toward isotropy and dual polarization better than a simple dipole.

With some interpretation of the UE patterns shown in the previous figures, we now look at a comparison of UE radiation patterns from the five sample UEs. They are shown in Figures 3.17 and 3.18. The first feature that stands out is the similarity in phones A, B, and C. These are different manufacturers with very different price points and dimensions. Yet, all three phones exhibit the same antenna behavior. Phones D and E, are similar to each other, but not the first three. They have a very different design. It may be that the design allows higher EIRP for most orientations while sacrificing some isotropy compared to the other antenna design. Another feature to note is the presence in all UEs of a 30-40 dB null in the pattern.

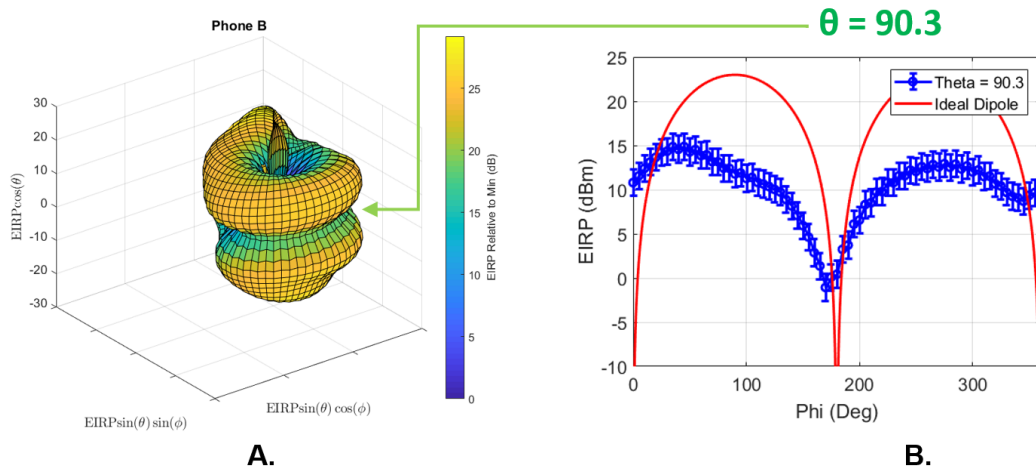


**Figure 3.14:** (A.) The three-dimensional antenna pattern of phone B with the measurement antenna horizontally polarized. The  $\theta$  direction is in the vertical plane of the figure, while the  $\phi$  direction is the horizontal plane. The measured EIRP is the color scale which is set to a relative scale so that the minimum measured is at 0 dB. (B.) The horizontal or  $\phi$ , cut taken at  $\theta = 90^\circ$  which is at the equator of the three-dimensional pattern, as indicated by the arrow. With this cut, the top of the phone is always cross polarized to the measurement antenna, leading to the waist seen at the equator of this pattern. The red curve represent the behavior of a simple dipole.

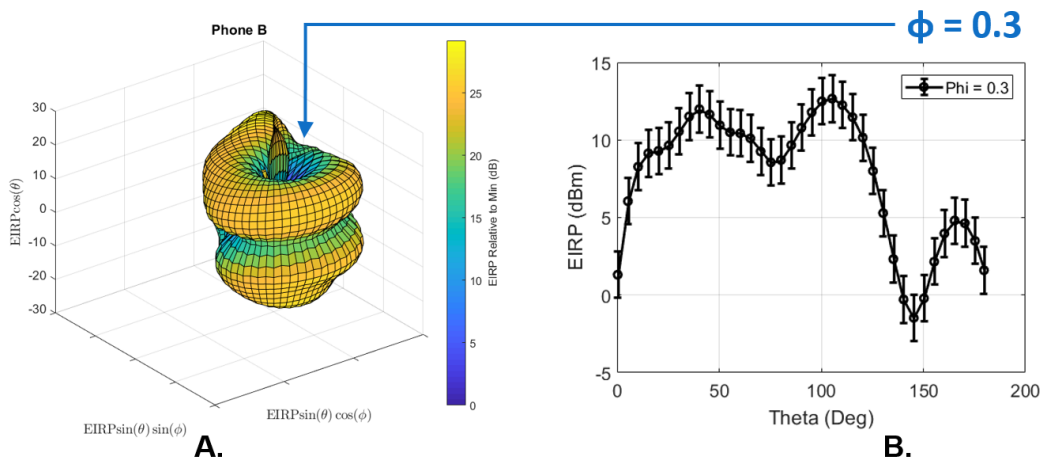


**Figure 3.15:** (A.) The three-dimensional antenna pattern of phone B with the measurement antenna horizontally polarized. The measured EIRP is the color scale which is set to a relative scale so that the minimum measured is at to 0 dB. (B.) The vertical, or  $\theta$ , cut taken at  $\phi = 0^\circ$  which starts at a null at the top of the three-dimensional pattern, as indicated by the arrow.

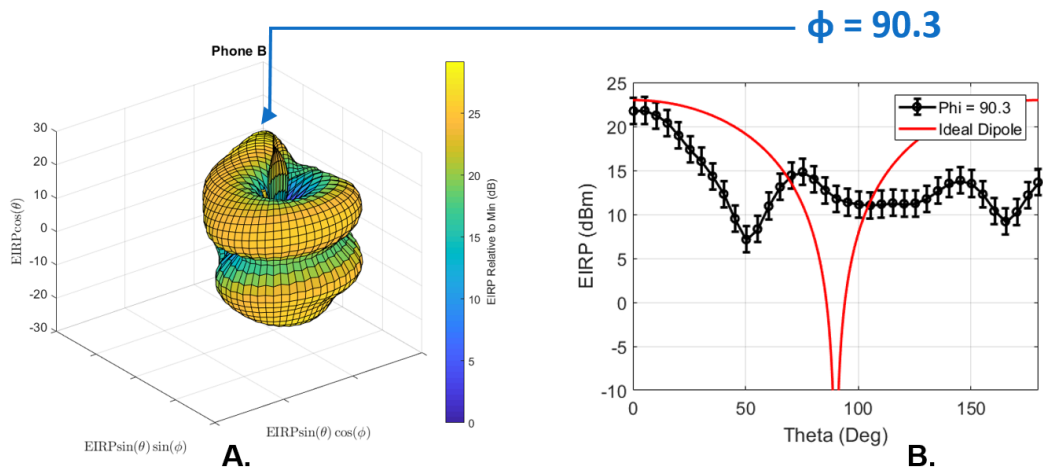


**Figure 3.16:** (A.) The three-dimensional antenna pattern of UE B with the measurement antenna horizontally polarized. The measured EIRP is the color scale which is set to a relative scale so that the minimum measured is at to 0 dB. (B.) The vertical, or  $\theta$ , cut taken at  $\phi = 90^\circ$  which starts at a peak in the radiation patten at the top of the three-dimensional pattern, as indicated by the arrow.

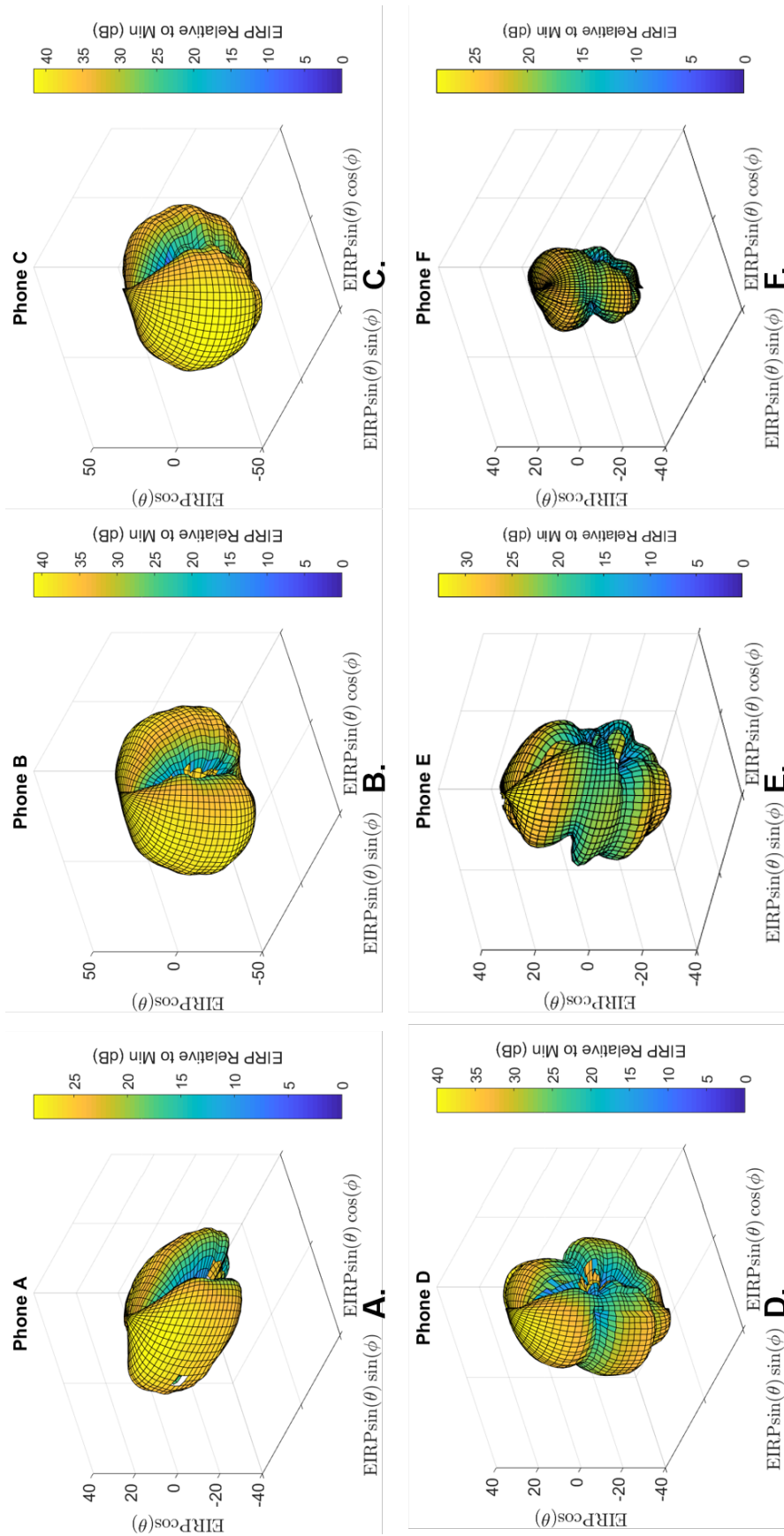


**Figure 3.17:** Three-dimensional radiation pattern with vertically polarized measurement antenna of (A.) phone A, (B.) phone B, (C.) phone C, (D.) phone D, (E.) phone E, (F.) phone F.

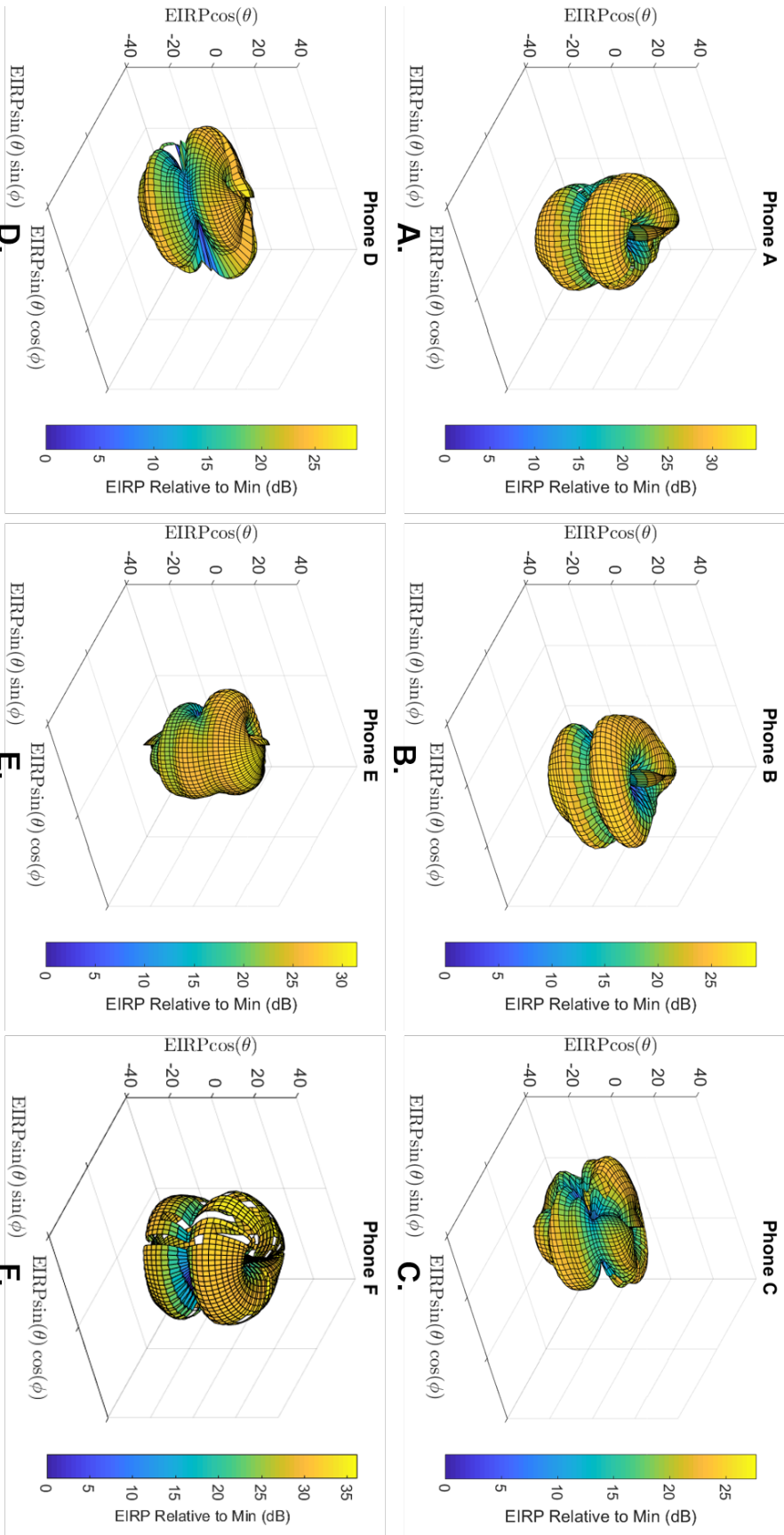


**Figure 3.18:** Three-dimensional radiation pattern with horizontally polarized measurement antenna of (A.) phone A, (B.) phone B, (C.) phone C, (D.) phone D, (E.) phone E, (F.) phone F.

# Chapter 4

## Discussion

### 4.1 Dipole Antenna Approximation

The antenna patterns measured on the UEs presented in this report have many features in their shape. In order to help interpret the behavior of the devices, we chose a dipole antenna as the first-order model. The validity of this choice can be seen in the data presented since the radiation patterns lend themselves to this approximation. Furthermore, the typical antenna used for wireless devices is approximately described, in relative gain, by an azimuthally symmetric dipole pattern [10].

We did not examine the antennas of each device, but generally, wireless devices use a so-called planar inverted F antenna (PIFA) design [10]. These antennas generally use the ground plane of the UE with a planar metal extension forming an L on one side. It could be thought of as a slot antenna with one open side. The feed for the antenna is between the ground plane and the arm of the L forming what looks like an inverted F, since the feed is typically close to the closed side of the open slot. These antennas are easy to fabricate and allow flexibility in impedance matching to 50 ohms across a large bandwidth, as compared to a monopole design antenna. With the correct dimensions chosen for this type of antenna, one can achieve an azimuthally symmetric pattern with an elevation dependence that matches the sinusoidal pattern of an ideal dipole pattern. The gain achieved will be quite different from a dipole, but the angular dependence will match. In actual devices, with dielectric material from the UE case present and with optimization for multiband or wideband operation, the radiation pattern can be expected to show multi-lobe behavior, but this can be viewed as a perturbation of the dipole model presented in this report [10].

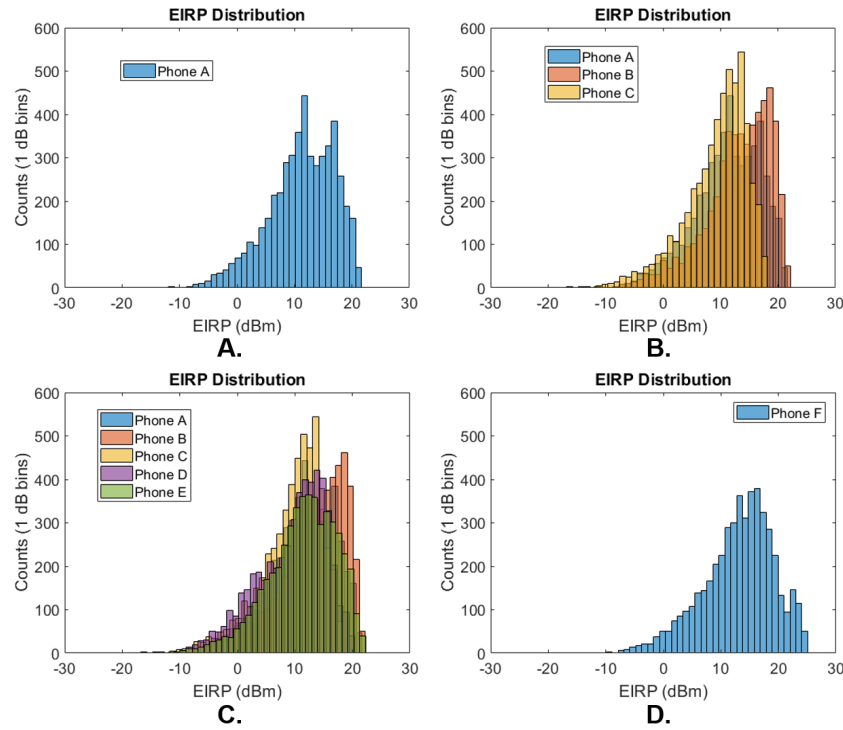


**Figure 4.1:** Histograms of the EIRP measured at all the angles with both horizontal and vertical polarization of the measurement antenna. A.) The histogram of only phone A. B.) Histogram of Phones A-C. C.) Histogram of Phones A-E for comparison D.) Histogram for phone F.

## 4.2 Distribution of EIRP

A goal of this report was to identify realistic power levels as a function of UE orientation to assist in maximizing measurement dynamic range and understanding associated uncertainties. Another useful metric when modeling the emissions (or aggregate emissions) of a UE is the distribution of power measured from the full UE patterns. These distributions could allow a better sense of the average interference power that will be seen by a victim device. Furthermore, the distributions provide an excellent source for a Monte Carlo sampling of expected power from the UE which could assist with understanding deviations from peak power. These distributions are shown in Figure 4.1. To ease with interpretation, distributions from the different phones are included in the four plots. Phones A-C show a sharp cutoff at their highest EIRP values. Phones D-F have histogram peaks at lower power, but have fewer points in the lowest-power regime. We speculate that their design is optimized to avoid the deepest nulls while sacrificing peak performance.

Additionally, the three-dimensional patterns shown all have the common feature of yielding 30 - 40 dB nulls in the patterns. In the case of interference calculations where the victim receiver's antenna of interest is dual-polarized, the sum of the patterns for horizontal and vertical polarization

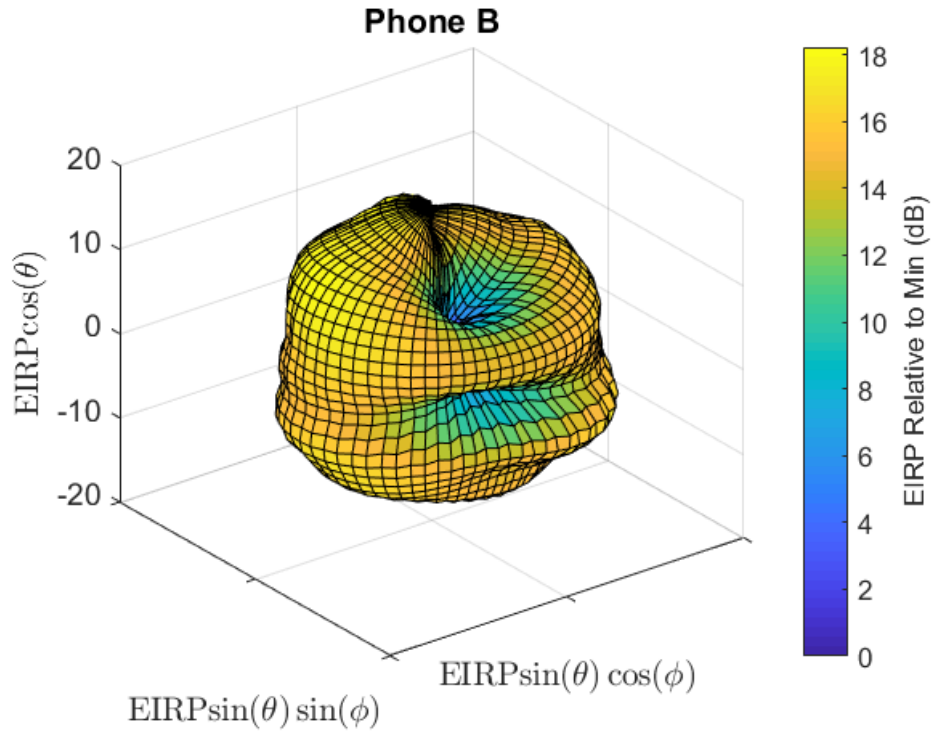


**Figure 4.2:** Three-dimensional pattern of sum of horizontal and vertical polarization of UE B

may be of more interest. In Figure 4.2, the pattern of the sum of polarization is shown. The nulls in this pattern are now 15-20 dB, which may better represent the actual power incident on a victim receiver.

# Chapter 5

## Conclusions

### 5.1 Summary

Here, we presented results in the form of antenna radiation patterns, histograms, and calculations from six handsets for use in the NASCTN LTE aggregate experiment. We discovered similarity in patterns and UE radiation behavior, including the effect of the data/power cable on the resulting pattern. From the patterns measured, we determined that 30 - 40 dB nulls are possible in all the handset patterns. Furthermore, the UEs tested here could be approximately modeled as a dipole co-linear with the top or bottom edge of the UE, yielding close to the maximum radiated output at that edge of the device when copolarized with the measurement antenna. However, when the charging/data cable for the UE was introduced, the repeatability of the location of peaks in the radiation pattern was reduced. Given these two results, we determined to use the top of the phone closest to and copolarized with the measurement antenna for the experiment at hand, which would also allow the length of the cable to be orthogonal to the measurement antenna polarization. This should give EIRP values within 1 dB of the maximum radiated power for all phones while allowing the best repeatability with cable placement and angular dependence.

# Appendix A

## Data Acquisition Flow

The UE patterns presented in this report were measured with a single antenna connected to a communications tester to both establish a communication link with the UE, and measure transmitted power from the UE. The advantage of this scenario is that there is not a second antenna, which would normally be used for establishing communication while the first antenna is attached to a spectrum analyzer for measuring transmitted power. The second antenna can distort the measured radiation pattern. However, the spectrum analyzer provides greater dynamic range in the power measurement. To overcome this limitation in the communications tester, the automation code was written to adjust the receiver range dynamically.

The communication tester has a setting called "external attenuation," which sets the receiver range for the expected incoming power. When this setting was substantially different than the expected channel loss, the tester would lose the communication link. In order to maintain the link, and therefore the power measurement, through nulls in the UE radiation pattern, several loops were coded to catch out of range errors. We changed the tester's external attenuation to implement this error handling.

A flow diagram of the data acquisition code is shown below in Figure A.1. There are three instruments automated: the turntable which yields the elevation angle, the rotation stage that yields the azimuth angle, and the communications tester, which produced all measurements shown in the diagram, except for the orientation angles. The measurements made were: EIRP; standard deviation of the EIRP measurement across the LTE frames averaged; attenuator setting (range of the receiver); timestamp when the data was written; an error code from the EIRP measurement that indicates whether the communication link was out-of-sync; the power was saturated, or if no error occurred; and finally the orientation of the rotation stages. We also recorded the reference signal received power (RSRP) from the UE. Finally, the communications tester reports an estimate of the UE transmit power, which is the power received on the port of the tester with the addition of the estimated path loss which is input as the attenuator setting. We were interested in the received power at the port of the tester so that we could apply our own, measured, path loss correction.

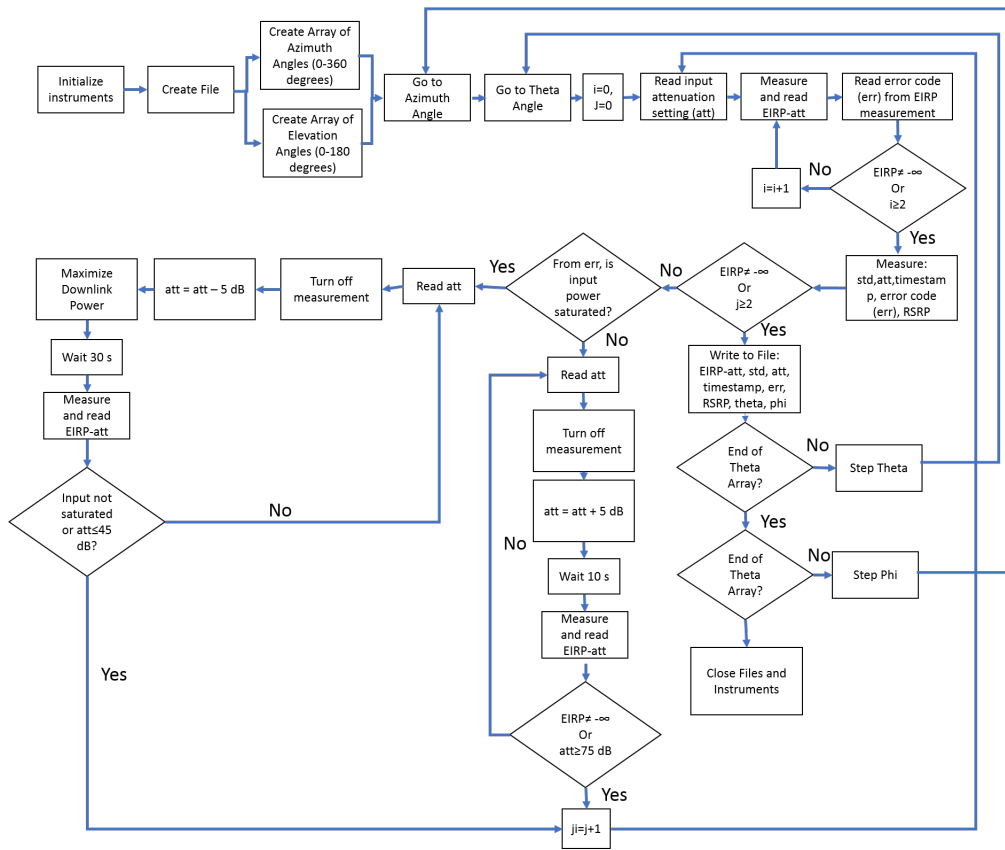


Figure A.1: Flow diagram of the data acquisition software.

The rotating stages, for both elevation and azimuth, were set to rotate at one revolution per minute. Thus, for the five degree steps, the time to rotate each stage was 0.8 s. The measurement would then commence and lasted a duration of approximately 5 s. Therefore, when a communication link was maintained, a measurement step would last 6 s. For a given azimuth angle, we would step through all the elevation angles, as depicted in figure A.1. In order to save time, the acquisition would alternate between measuring increasing elevation angles from 0 ° to 180 °, step to the next azimuth angle, then reverse the elevation step to measure decreasing angles. Additional testing time would be required when the communication link was lost due to high path loss, or due to power saturation. As is shown in figure A.1, if connection was lost due to lack of signal, the external attenuation setting would be decreased by 10 dB and a pause of 10 s was added to allow reacquisition of the LTE signal. The valid range found for the attenuation setting in the chamber was 45-75 dB, allowing a possibility of 4 attempts at reestablishing the communication link. Thus, those data points could require up to 40 s for acquisition when a low signal was encountered. Also, since finding a null in the pattern would yield a high attenuation setting, once the UE was at an angle that was out of the null, we would find the communication tester receiver saturated. This would be indicated by an error code from the tester. Then the attenuation setting would be decreased, but we found that acquiring the LTE signal could take up to 30 s. Therefore, with the possible four steps of attenuation attempts, these points could take up to 2 min to acquire.

The UE patterns were measured at 5 ° increments for pinpointing the presence of nulls in the pattern. This step size required 72 data points in the azimuth angle, and 36 points in the elevation angle. Therefore, a total of 2592 angular configurations were measured. If the communication link were maintained throughout, one would expect at 6 s per data point, to acquire a pattern, for a given measurement antenna polarization, in 4.3 hours. However, a typical pattern required 6 hours due reestablishing the signal from low power or saturation.

# Bibliography

- [1] GPO. Presidential memorandum: Unleashing the wireless broadband revolution. [Online]. Available: <https://www.gpo.gov/fdsys/pkg/CFR-2011-title3-vol1/pdf/CFR-2011-title3-vol1-other-id236.pdf>
- [2] NTIA. An assessment of the near-term viability of accommodating wireless broadband systems in the 1675-1710 mhz, 1755-1780 mhz, 3500-3650 mhz, and 4200-4220 mhz, 4380-4400 mhz bands. [Online]. Available: [https://www.ntia.doc.gov/files/ntia/publications/fasttrackevaluation\\_11152010.pdf](https://www.ntia.doc.gov/files/ntia/publications/fasttrackevaluation_11152010.pdf)
- [3] FCC. Amendment of the commission's rules with regard to commercial operations in the 1695-1710 mhz, 1755-1780 mhz, and 2155-2180 mhz bands, fcc report and order, fcc 14-31. [Online]. Available: [https://transition.fcc.gov/Daily\\_Releases/Daily\\_Business/2014/db0401/FCC-14-31A1.pdf](https://transition.fcc.gov/Daily_Releases/Daily_Business/2014/db0401/FCC-14-31A1.pdf)
- [4] ——. Auction 97, advanced wireless services (aws-3). [Online]. Available: [http://wireless.fcc.gov/auctions/default.htm?job=auction\\_summary&id=97](http://wireless.fcc.gov/auctions/default.htm?job=auction_summary&id=97)
- [5] DSO, "Advanced wireless services-3 early entry portal analysis capability algorithm definition document," vol. DSO-HDBK-16-097, 2016.
- [6] A. Ghosh, "Lte uplink analysis," in *CSMAC*. CSMAC, 2012.
- [7] CTIA Certification, *Test Plan for Wireless Device Over-the-Air Performance, Method of Measurement for Radiated RF Power and Receiver Performance*, Washington, DC, Feb. 2018, version 3.7.1. [Online]. Available: <https://www.ctia.org/initiatives/certification/certification-test-plans>
- [8] DSO, "Spectrum sharing test and demonstration (sstd) lte performance and emissions characteristics," vol. DSO-TN-17-003, 2017.
- [9] J. Kraus, *Antennas*, 2nd ed. Boston: McGraw-Hill, 1988.
- [10] P. Hall, E. Lee, and C. Song, *Printed Antennas for Wireless Communications*. New York: John Wiley & Sons, 2008, ch. Planar inverted-F antennas.